Erosion of steepland valleys by debris flows

Jonathan D. Stock†
U.S. Geological Survey, Menlo Park, California, USA

William E. Dietrich
Earth and Planetary Science, University of California, Berkeley, California, USA

ABSTRACT

Episodic debris flows scour the rock beds of many steepland valleys. Along recent debris-flow runout paths in the western United States, we have observed evidence for bedrock lowering, primarily by the impact of large particles entrained in debris flows. This evidence may persist to the point at which debris-flow deposition occurs, commonly at slopes of less than ~0.03–0.10. We find that debris-flow–scoured valleys have a topographic signature that is fundamentally different from that predicted by bedrock river-incision models. Much of this difference results from the fact that local valley slope shows a tendency to decrease abruptly downstream of tributaries that contribute throughgoing debris flows. The degree of weathering of valley floor bedrock may also decrease abruptly downstream of such junctions. On the basis of these observations, we hypothesize that valley slope is adjusted to the long-term frequency of debris flows, and that valleys scoured by debris flows should not be modeled using conventional bedrock river-incision laws. We use field observations to justify one possible debris-flow incision model, whose lowering rate is proportional to the integral of solid inertial normal stresses from particle impacts along the flow and the number of upvalley debris-flow sources. The model predicts that increases in incision rate caused by increases in flow event frequency and length (as flows gain material) downvalley are balanced by rate reductions from reduced inertial normal stress at lower slopes, and stronger, less weathered bedrock. These adjustments lead to a spatially uniform lowering rate. Although the proposed expression leads to equilibrium long-profiles with the correct topographic signature, the crudeness with which the debris-flow dynamics are parameterized reveals that we are far from a validated debris-flow incision law. However, the vast extent of steepland valley networks above slopes of ~0.03–0.10 illustrates the need to understand debris-flow incision if we hope to understand the evolution of steep topography around the world.

Keywords: geomorphology, erosion, debris flows, river incision, landscape evolution.

INTRODUCTION

In steeplands, landslides within hollows may mobilize into debris flows that scour down valley networks, superficially resembling those cut by streams (Fig. 1). Some have argued that this steep network is lowered during debris flows by processes fundamentally different from those of bedrock river incision (Seidl and Dietrich, 1992; Montgomery and Foufoula-Georgiou, 1993; Sklar and Dietrich, 1998; Snyder et al., 2000; Stock and Dietrich, 2003). These workers proposed that there is a scaling break in logarithmic plots of valley drainage area against slope, signifying the transition between debris flow or hillslope processes, and fluvial ones. The break is commonly defined as the uppermost valley slope at which data still follow a linear fluvial trend, and is often reported to occur at drainage areas of ~0.1–1 km^2. Some have proposed that the trend of area-slope data above the scaling break is also log-log linear, differing only from those of rivers by a lower concavity (e.g., Whipple and Tucker, 1999; Lague and Davy,

Figure 1. Debris-flow valley network in an Oregon Coast Range clear-cut. The combination of elevated water pressure during a 1996 storm and reduced root strength initiated landslides at valley heads that mobilized as debris flows, scouring sediment and the Eocene Tyee sandstone (white areas) along the runout. Road at top right indicates scale.

†E-mail: jstock@usgs.gov.

GSA Bulletin; September/October 2006; v. 118; no. 9/10; p. 1125–1148; doi: 10.1130/B25902.1; 18 figures; 5 tables.

2003). For instance, on the basis of 90 m digital elevation model (DEM) data from Nepal, Lague and Davy (2003) proposed an incision law for "colluvial" valleys that is similar to bedrock river-incision laws.

Stock and Dietrich (2003) found that valleys traversed by debris flows have a plot of slope against drainage area that is curved in log-log space, so long as data are measured from sufficiently high-resolution contour maps or DEMs. They found that valleys with curved area-slope plots corresponded to the part of the valley network where they observed evidence for debris-flow incision, often at slopes above ~0.03–0.10. It is likely that at many slopes between ~0.03 and 0.10, valley incision occurs by a combination of river and debris-flow incision (Stock et. al, 2005). However, the network remaining above ~0.10 slopes comprises most of the steepland relief (e.g., 25%–100%) and network length (e.g., >80%) in many watersheds. In this part of the landscape, most sediment first transits a debris-flow valley before arriving at a river. Most hillslopes in these steep landscapes are bounded by debris-flow valleys, whose lowering rate they must approach at long time scales. An outstanding implication is that much of the steepland response to river incision, both as growth and decay of topography, is probably conditional upon debris-flow valley incision.

For this reason, a debris-flow incision law needs to be part of future landscape evolution models. However, a wide variety of solid and fluid stresses can occur during an individual debris flow (e.g., Iverson, 1997), and it may be difficult if not impossible to reduce these to one erosion law in the absence of further guidance. In this article we use field observations that point toward the relevant stresses that lower rock to provide some justification for a simplified approach. Storms in California, Oregon, and Washington during the middle to late 1990s initiated many debris flows (e.g. Figs. 1, 2), providing an opportunity to view widespread evidence for bedrock erosion by debris flows.

We hypothesize a model of debris-flow incision that is based on field evidence from 16 of these recent debris flows for the mechanics of rock lowering by debris flows, the bulk debris-flow stresses associated with such lowering, and the role of network structure and weathering. These observations are largely from soil-mantled landscapes with coarse, granular debris flows that initiated as landslides during storms (e.g., Fig. 2), so the resulting model is most appropriate to such sites. It is not intended to represent landscapes where debris flows or hyper-concentrated flows initiate by runoff and sediment bulking up (e.g., Cannon, 2001; Meyer et al., 2001).

Figure 2. Coarse-grained debris-flow front in Valley of the Falls, San Bernardino Mountains, California, 3 days after deposition on 13 July 1999. Median diameter of boulders is ~0.3 m. Such coarse boulder fronts are characteristic of many sites we investigated (Table 1).

Figure 3 illustrates one view of the problem. A landslide mobilizes from a hollow as a debris flow that translates down the long-profile, increasing in length as it entrains colluvium from the valley bottom, but slowing down (smaller arrows) as the slope declines. We hypothesize that as the flow slows down, bedrock lowering from the impact stresses of large particles decreases. However, as the flow entrains coarse colluvium from the valley floor, it grows in length, counteracting the reduction in erosion from lower-impact stresses. On the basis of field observations summarized later, we hypothesize that flow depth does not grow substantially along the runout path. Over the course of many events, the valley network structure controls the number and size of debris flows through the main stem illustrated in Figure 3. Observations indicate that debris flows that follow pathways without sharp junction angles are preferentially mobile. For many valley networks, these field observations predict that the long-term frequency of debris-flow events should increase rapidly down the main stem in the headwater reaches, and more slowly in the lower basin, where tributaries tend to enter at acute angles that do not convey events to the main stem. We hypothesize that as the number of debris-flow events increases down a valley, reach slope and average degree of bedrock valley floor weathering decrease over the course of many events toward values that equilibrate network lowering rates. Specifically, we hypothesize that reductions in reach slope lower impact velocities and reduce event lowering, whereas reductions in elapsed time between events decrease rock weathering, and consequently event lowering.

We use these hypotheses to guide field studies and to develop a first approximation for a geomorphic transport law for debris-flow incision that is consistent with field observations. Consequently, the proposed geomorphic transport law (*sensu* Dietrich et al., 2003) is meant to capture some of the essential properties that are likely shared by many debris-flow networks, and to serve as a hypothesis to guide future flume, field, and modeling efforts.

FIELD SITES

On an opportunistic basis, we visited valleys with recent (<2-yr-old) debris flows in the western United States (Table 1; Stock, 2003) over the period 1996–2000. These flows were largely triggered by landslides, many of which initiated at hillslope hollows during intense rainfall, a process that has been studied extensively on soil-mantled landscapes (e.g., Dietrich and Dunne, 1978; Dietrich et al., 1986; Iverson and Major, 1986; Reneau and Dietrich, 1987). The resulting flows were composed of water and a wide range of grain sizes, including many boulders preserved in terminal flow deposits and levees, commonly from several to tens of meters long.

In southern California, intense thunderstorms during 11 and 13 July 1999 triggered debris

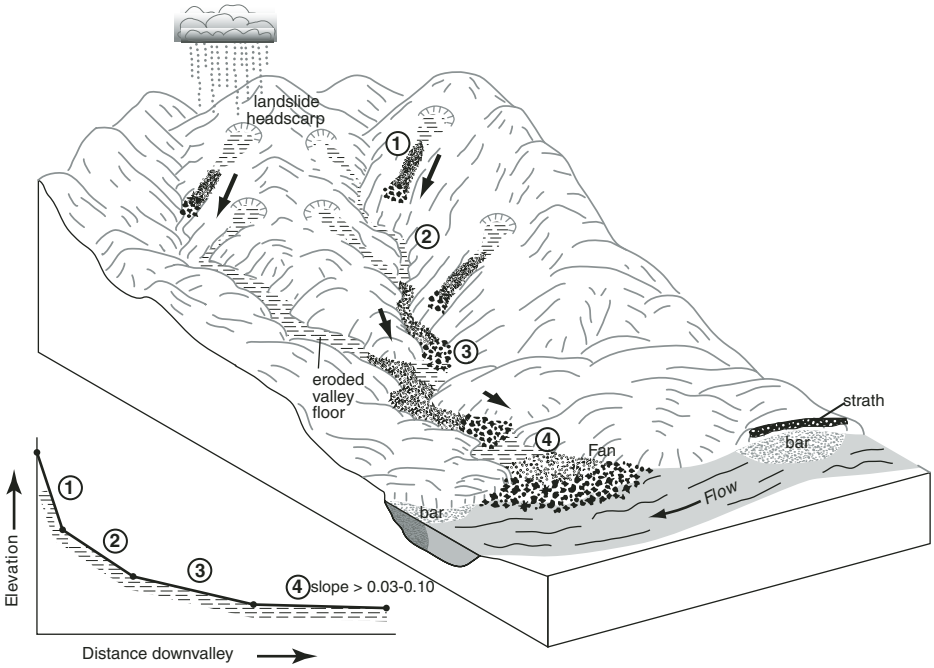

Figure 3. A view of debris-flow incision. As individual debris flows mobilize from rainfall-induced landslides in hollows, they erode valley floors (dashed pattern), slow down as slopes decrease (reduction in arrow length), and grow in length as they entrain material from the valley floor (increases in dark particles representing coarse, erosive flow fronts). This time-transgressive cartoon is meant to illustrate the network pattern of debris-flow properties that might lead to the inset hypothetical long-profile, with its abrupt reductions in valley slope below tributaries that contribute mobile debris flows. In this view, fast, frequent flows with long, granular snouts erode a valley network that is largely above slopes of 0.03–0.10, below which granular flows are rarely mobile. At lower slopes, fluvial processes dominate transport of sediment (e.g., bars) and bedrock lowering (strath terraces). As illustrated in the picture, most of the relief of many steeplands is composed of valley networks cut by episodic debris flows.

flows along the southern margin of the Valley of the Falls, San Bernardino Mountains. Boulders in coarse-granular debris-flow fronts (Fig. 2) moved rapidly across fans at the base of Yucaipa Ridge, killing two people. Three days later, we walked a large runout at the northern extremity of the town (Yucaipa in Table 1) where a boulder-rich debris flow had scoured garnet mica schists exposed on the valley floor near the fan head. Cliffs along the valley prevented access to the initiation source on Yucaipa Ridge, which is estimated to be lowering at ~1 mm/yr on the basis of U/Th–He data (Spotila et al., 1999).

In the Bear River headwaters of the San Gabriel Mountains, we investigated the runout of two recent debris flows whose sand and boulder levees were still dewatering during our visit. The 13 July thunderstorm the previous day likely triggered these events. Along runouts, we observed local abrasion and block-plucking of the Mesozoic granite and diorite valley floor and removal of preexisting talus piles in and along valleys. Downstream of recent debris-flow deposits, boulder fields from older debris-flow deposits filled the length of the valley for several hundred meters. Farther below, potholes and runnels mark the first widespread occurrence of fluvial features, and the beginning of area-slope data that are log-log linear (Stock and Dietrich, 2003). Erosion rates in this part of the San Gabriel Mountains are ~1 mm/yr on the basis of apatite fission-track data (Blythe et al., 2000). Nearby cosmogenic radionuclide samples (Stock, 2003) indicate that debris flows are incising valley bottoms at rates of 0.75 mm/yr, a value that is not statistically different from catchment-wide rates of 0.75 mm/yr estimated from channel sands.

Winter storms in 1996–1997 triggered hollow failures and subsequent debris flows above Highway 9 in the forested Santa Cruz Mountains of northern California. We investigated a flow that scoured Neogene arkose along its runout, plucking fractured blocks from the valley bed. Erosion rates on the adjoining western side of the range are ~0.2–0.3 mm/yr, as estimated from sediment yield (Brown, 1973) and cosmogenic radionuclide analysis of sediment (Perg et al., 2000). A debris flow to the north, along Pescadero River, also occurred during the 1996–1997 storms, and we visited it to examine evidence for rock weathering. In the northern California Coast Range near Scotia, we walked the runout of a large debris flow that destroyed houses adjacent to Highway 101. A landslide at the valley head mobilized as a debris flow that lowered chert and sandstone cropping out along the valley floor.

Utah State Geological Survey personnel alerted us to a 1997 debris flow that scoured Joe's Canyon in the Paleozoic Oquirrh Formation (Davis, 1983), a quartzose sandstone in the foothills of the Wasatch Range near Spanish Forks, Utah. When we walked the channel, it was dry and lacked exposures of sorted sediment, defined channel banks, or fluvial features like potholes or plunge pools. We observed decimeter-sized blocks missing from the jointed quartzite bedrock of the valley bed, along with widespread abrasion marks. Long-term erosion rates in the vicinity of the Salt Lake City segment to the north are ~1–2 mm/yr on the basis of fission-track and U/Th–He data (Armstrong et al., 1999).

Winter 1996–1997 storms initiated landslides throughout the Oregon Coast Range, many of which mobilized as debris flows that scoured sediment from valley floors and exposed carbonate-cemented sandstones and siltstones of the Eocene Tyee Formation (Walker and MacLeod, 1991; Ryu et al., 1996). High-resolution topography from laser altimetry (Fig. 4) covers two sites with recent debris flows adjacent to the southern (Sullivan) and northern (Scotsburg) boundaries of Elliot State Forest. The data quality rivals that of 1 m hand-level surveys for the same area, capturing variations in local valley slope that correlate with siltstone (dashed) or massive sandstone beds (Fig. 5). We also found older debris-flow deposits along Sullivan and Marlow Creeks (~1 km east of the area of Fig. 4). Valleys in Figure 4 have curved area-slope plots (Fig. 6), proposed by Stock and Dietrich (2003) as a signature for debris-flow incision. Within Elliot State Forest we also located debris flows in Marlow Creek, Silver Creek, and Elk Creek drainage basins. Marlow Creek sites initiated as landslides in hollows whose vegetation was predominantly second-growth alder with low total root strengths (Schmidt et al., 2001; Roering et al., 2003). The debris flow at Silver Creek occurred in a recent clear-cut. Those in Elk Creek occurred in second-growth forest with low-stand densities. Long-term erosion rates in the Sullivan basin are estimated at ~0.1 mm/yr on the basis of sediment yield and hollow accumulation rates (Reneau and Dietrich, 1991) and cosmogenic radionuclides

TABLE 1. CALCULATIONS BASED ON FIELD OBSERVATIONS

Location	Site	Date of event	Lithology	Erosion Features	Median folia (mm)	Length **total** /xs (m)	% bed -rock	Slope	Width (m)	Depth max. (m)	Velocity (m/s)	Peak flux (m^3/s)	Trigger link magnitude N_t	D_{50} boulders (m)	Deposit volume (m^3)	Bulking (m^3/m)	Static solid normal stress (kPa)	Inertial solid stress (kPa)
Olympics, WA	FR 23 (3 pin xs)	1997?	diabase	abrasion, folia, block-plucking	8	**533** / 52	70	0.51	9.5	2.7			2	0.2	9990	17.0	37.5	
	"	"	"	"	18	188		0.36	11.0	3.8			3	0.2			55.6	
Oregon	Silver Creek	1996	med. ss (Tyee)	abrasion, folia, grooves, block-plucking		**>220** /60	100	0.33	3.4	1.6			-	?			23.7	
Coast Range	ODF#535	1996	"	"		**303** /201	69	0.28	9.0	2.5	7.6		>3	0.4	-		37.5	2.3
	ODF#733	1996	"	"		**272** /53	59	0.38	12.3	4.7	6.6		>2	0.3	-		69.0	0.3
	Marlow1	1996	"	abrasion, folia,		**700** /353	42	0.23	12.5	5.5			7	0.3	6000 ± 2000	7.5	83.3	
			"	block-plucking		288		0.32	7.7	3.1			5				46.3	
			"	"		281		0.32	9.2	3.8			5				55.9	
			"	"		273		0.29	9.5	4.5			5				66.8	
			"	"		266		0.29	12.4	5.6			5				83.7	
			"	"		259		0.29	14.0	6.0			5				90.1	
			"	"		252		0.27	14.1	5.0			5				74.5	
			"	"		244		0.27	14.1	5.0			5				74.6	
			"	"		237		0.29	12.1	4.9			5				73.9	
			"	"		230		0.29	11.3	4.7			5				70.8	
			"	"		223		0.29	11.6	4.4			5				66.2	
			"	"		216		0.36	10.7	4.5			5				66.3	
			"	"		209		0.36	11.2	5.7			5				82.9	
			"	"		201		0.19	9.1	3.8			5				58.8	
			"	"		159		0.46	9.8	4.2			4				59.6	
	Marlow 2	1996	"	"		**491** /370	77	0.17	13.0	2.6			8	0.7	~800	0.3	39.9	
			"	"		326		0.14	16.0	2.4			8				37.0	
			"	"		122		0.27	12.0	2.5			4				37.6	
			"	abrasion, folia, grooves		66		0.55	12.0	2.0			3				27.3	
			"	abrasion, folia, block-plucking		38		0.39	11.0	2.5			3				36.3	
	Marlow 3	1996	"	"	7	**244** / 238	76	0.12	16.0	5.4			>2	0.3	660 ± 200	1.0	83.5	
	(10 pin xs)		"	"	6	14		0.49	12.6	3.8			>2				53.2	
	Marlow 4	1996	"	"	4	**192** /150	70	0.60	6.7	3.2			>2	0.3	135	0.03	43.2	
	(8 pin xs)		"	"	4	143		0.60	7.3	3.6			>2				48.7	
			"	"	4	135		0.17	6.6	3.3			>2				50.6	
			"	"	4	128		0.17	8.3	3.7			>2				56.1	
			"	"	4	121		0.30	8.4	3.5			>2				51.7	
			"	"	7.5	114		0.30	7.9	4.0			>2				60.3	
			"	"	4	106		0.28	6.4	3.5			>2				52.9	
			"	"	4	99		0.28	8.4	3.5			>2				53.2	
			"	"	4	92		0.32	9.4	3.5			>2				52.3	
			"	"	4	85		0.32	9.4	3.5			>2				52.6	
			"	"	4	78		0.33	11.1	3.8			>2				55.7	
			"	"	4	71		0.33	7.8	3.0			>2				44.9	
			"	"	4	64		0.32	7.0	2.8			>2				40.9	
			"	"	4	57		0.32	6.7	3.2			>2				48.0	
			"	"	4	50		0.41	9.1	3.8			>2	0.3			55.4	
	Sullivan 1	1996	"	abrasion, folia, grooves, block-plucking	7	**1070** /582	76	0.07	9.0	3.0	5.8		15	0.3	~1100	1.0	46.6	1
	Rock Cr. #1	1996	med. ss	abrasion, block-plucking		**1510** /212	~45	0.50	11.0	4.1	9.0	180	>10	0.5	2185–5395	2.5	56.4	2
	#2		(Yamhill Fm.)	soil scour		515		0.06	19.0	2.8	7.8	150	>10	0.5			43.6	3
	#3		"	soil scour		739		0.20	16.0	6.1	9.7	90	>10	0.5			93.2	1
	#4		"	abrasion, block-plucking		800		0.16	16.8	4.6	9.0	280	>10	0.5			70.8	2
	#5		"	abrasion, block-plucking		921		0.30	13.1	6.6	8.2	260	>10	0.5			97.8	1
	#6		"	soil scour		990		0.20	31.0	3.9	11.6	270	>10	0.5			58.8	4
	#7		"	soil scour		1000		0.07	40.0	5.3	7.2	450	>10	0.5			82.4	1
	#8			soil scour		1176		0.11	32.0	4.0	5.9	240	>10	0.5			62.0	1
Coast Range, CA	Scotia	1997	chert	abrasion, block-plucking		?	?	0.55	>5	>3			>10	<0.1				
S. Cruz Mtns., CA	Hiway9	1996?	arkose	abrasion, block-plucking		**>109** / 27	77	0.45	10.2	4.0	6.4	160	2	0.5			56.8	1
Wasatch, UT	Joe's #1	1998	quartzite	abrasion, block-plucking		**1590** /715	38	0.09	9.0	4.5	6.4	55	>10	0.4	1835	0.9	69.8	1
	#2		"	"		1135		0.13	8.5	3.0	5.9	100	>10	0.4			46.4	1
San Gabriels, CA	Bear Cr.	1999	granodiorite	abrasion, block-plucking		?	?	0.15	5.1	1.6	5.1	25	>10	0.5			24.7	4
	"	"	"	"		?	?	0.25	5.0	1.7	3.9	46	>10	0.5			25.7	2
	Redbox	1998?	"	abrasion, block-plucking		**>225**	100	>0.21	>4	>2			>7	<0.2				
San Bernardino, CA	Yucaipa	1999	garnet schist	abrasion, block-plucking		**>1000**	?	>0.31	>10	>4	>8.1		>10	0.3	~4800			

Note: Slope from inclinometer; width estimated from trimlines; velocity from equation 1; depth from field estimate of thalweg to trimline; static normal stress estimated using $\rho = 2560$ kg/m^3, and assuming solids volumetric fraction of 0.6 under dry conditions; inertial stresses calculated using equation 5, assuming $\partial u/\partial z \sim u_s/$ depth and assuming solids volumetric fraction is 0.6.

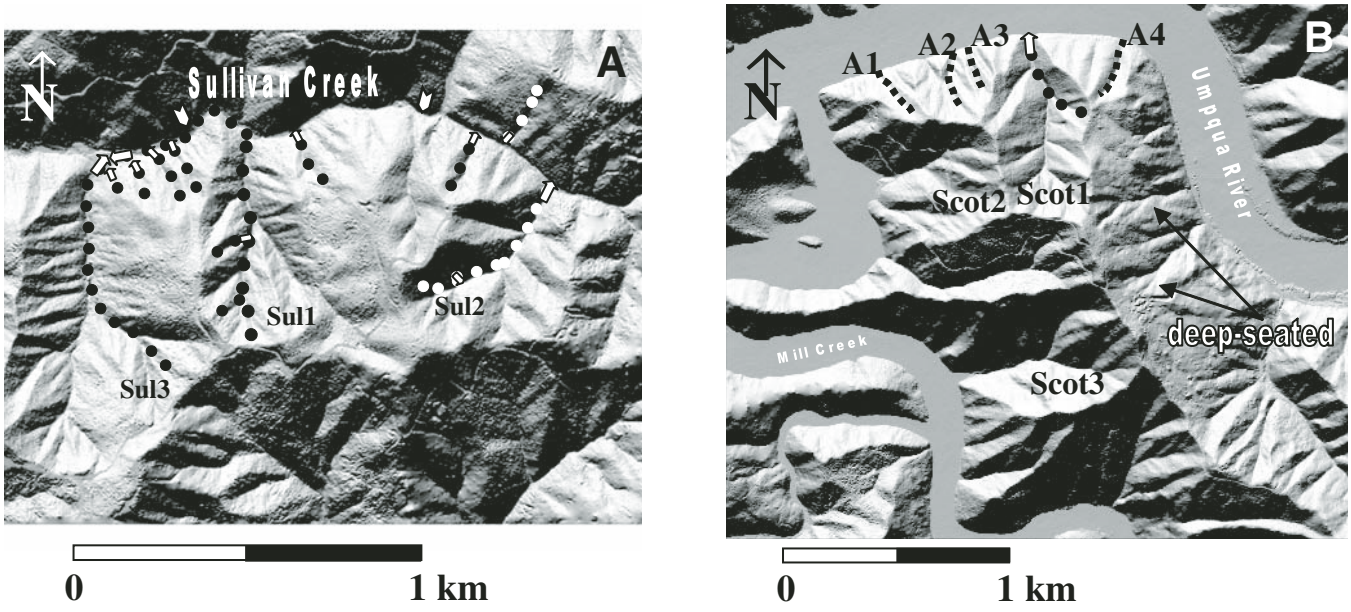

Figure 4. Shaded-relief images of high-resolution airborne laser altimetry from Oregon at Coos Bay (left) and Scotsburg (right) used to calibrate incision model. Black and white dotted lines indicate 1996–1997 debris flows and associated rock lowering, as mapped in the field. (A) Large arrows indicate terminal deposits of debris flows that transited main-stem valleys; small arrows indicate debris flows that were deposited where junction angles were >60°. In this shaded-relief image of Sullivan Creek, average topographic data spacing was 2.5 m with ~0.3 m vertical resolution. Wide arrows along the valley at the top of this panel bracket a knickpoint on Sullivan Creek. Note the less dissected landscape upvalley from the knickpoint. (B) Scotsburg area, in which average topographic data spacing was 4 m with ~0.3 m vertical resolution. Dashed lines labeled A1–4 correspond to valleys in Figure 10. Hillslopes draining to Sullivan Creek from the top part of the image are likely deep-seated failures (as judged by the lack of larger valleys), so we chose not to use them for analysis. Deep-seated landslides also occur in the northeast quadrant of this panel and are a process whose occurrence in this region is in part structurally controlled (Roering et al., 1996).

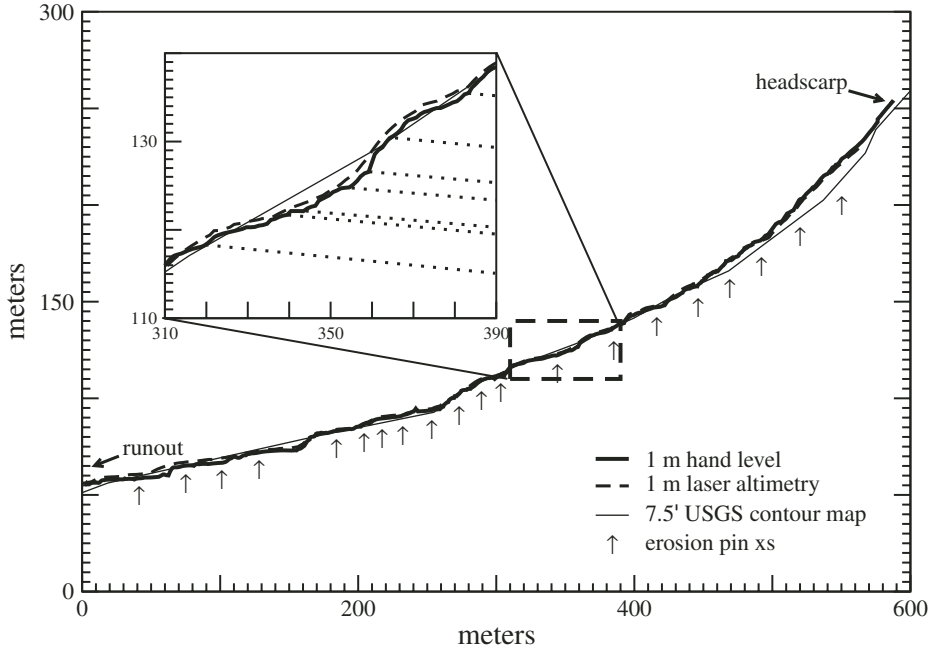

Figure 5. Comparison of laser altimetry long-profile to 1 m hand level and U.S. Geological Survey 7.5-minute quadrangle topography for Sul1. Inset illustrates influence of alternation between massive sandstone and siltstone (dashed lines) on local slope, and the accuracy with which laser altimetry captures such fine-scale variation. Erosion pin cross sections (xs) shown by arrows.

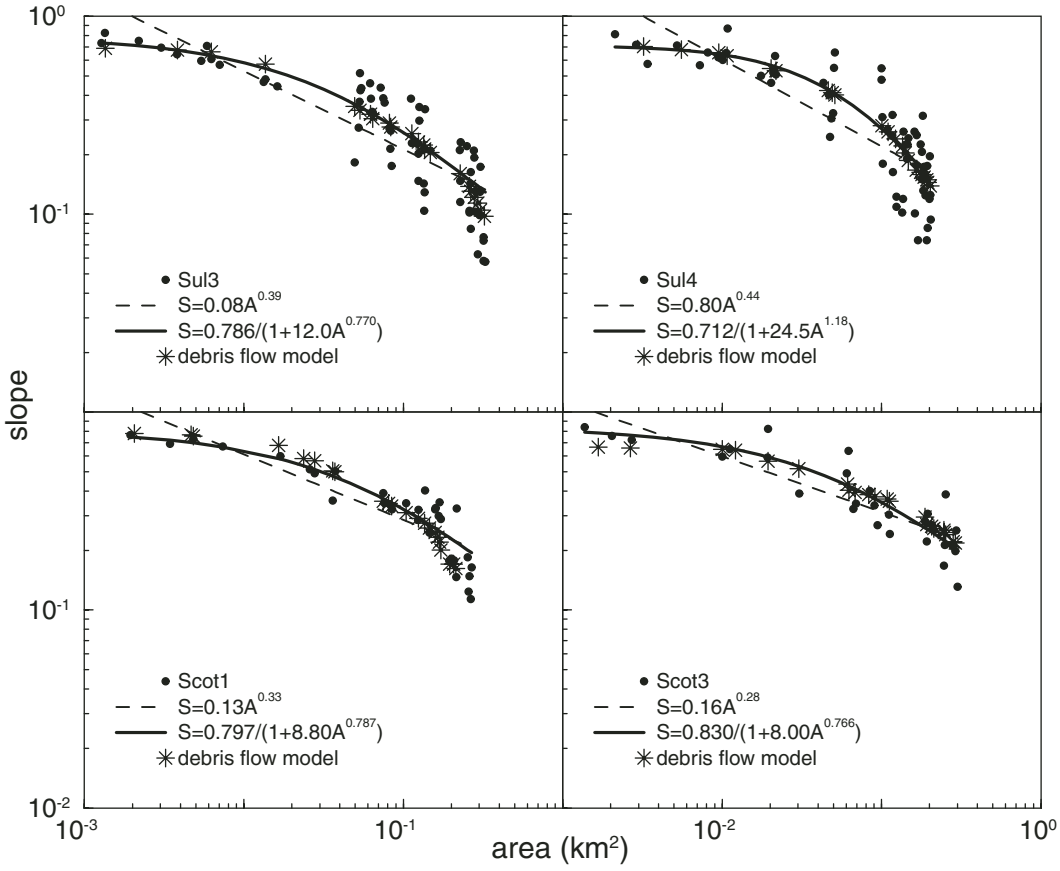

Figure 6. Area-slope data for the valleys scoured by debris flows in Figure 4 are unequivocally nonlinear. Linear power law regressions (dashed) are shown for comparison and are used to simulate fluvial long-profile evolution in Figure 18. Solid lines indicate curved empirical fits to data from equation 5 from Stock and Dietrich (2003). Slope-area data (asterisks) from steady-state debris-flow incision models in Figure 18 reproduce much of the curvature of the existing long-profiles.

(Heimsath et al., 2001). Lowering rates near the Scotsburg site are estimated at ~0.2 mm/yr from radiocarbon dates on strath terraces (Personius, 1995). Reneau and Dietrich (1991) proposed that the correspondence between sediment yield and hollow accumulation rates in Sullivan Creek is evidence for approximate steady-state lowering in this basin.

In Washington State, we walked a debris flow that scoured Eocene Crescent Formation basalts on the southern margin of the Olympic Mountains, near U.S. Forest Service Road 23 (Table 1). The landslide headscarp occurred in 7-m-deep glacial deposits, associated with Pleistocene valley glaciers. Old-growth Douglas fir and cedar forest covered the land prior to historic clear-cutting in the first half of the twentieth century. A fission-track study by Brandon et al. (1998) indicates Neogene exhumation rates of <1 mm/yr in the metasedimentary core of the Olympics that diminish outward to <0.3 mm/yr in the flanking basaltic and sedimentary rocks.

METHODS

In the following paragraphs we describe field methods and calculations that we used to estimate the bulk flow stresses accompanying debris-flow incision of bedrock at field sites reported in Table 1. The field observations are intended to lead to a simplified debris-flow incision law by connecting observations of bedrock lowering with the dominant stress causing them. We recorded different styles of bedrock lowering, and measured boulder sizes in some terminal levees. At sites selected for uniform lithology, we also measured bedrock weathering properties and fracture spacing.

Field Surveying

To record width, slope, and bedrock lowering by recent debris flows, we surveyed valley bottom profiles at 10 m increments with tape and inclinometer, and locally by hand level at meter intervals. We measured debris-flow width and maximum depths using preserved trimlines, and mapped the location of scoured bedrock and debris-flow deposits. Where possible, we estimated bulking rates (the incremental volume added per unit of distance traveled) by measuring initial landslide volume, final debris-flow-deposit volume, and runout distance. We used debris elevation differences between the upstream and downstream sides of trees (Δh) to estimate rough streamwise peak-flow surface velocity u_s:

$$u_s = (2\alpha g \Delta h)^{0.5}, \quad (1)$$

where the velocity head coefficient α is assumed to be 1 in the absence of field data on velocity gradients for coarse-grained debris flows, and g is the gravitational constant. Experimental testing of this approach (Iverson et al., 1994) indicates that velocities back-calculated from equation 1 can be as low as half of measured surge velocities. Surviving trees are commonly nearer to the low-velocity margins of the flow, further biasing estimates to low values. We cite debris-flow velocities in Table 1 as representative, if imprecise, estimates of streamwise velocity.
Table A1 lists the various characters and symbols used in this article.

Estimation of Debris-Flow Stresses

Field and experimental evidence indicates that many debris flows are characterized by coarser-grained, fluid-poor surge heads (e.g., Fig. 2) and finer-grained, fluid-rich interiors (see Iverson, 1997). Static and inertial solid stresses

are high in coarse flow fronts; fluid stresses and solid-fluid interaction stresses characterize the finer-grained interior. Iverson (1997) argued that no single rheology can capture these variations, so that much previous work on rheology cannot be applied to bulk flows. We propose that back-calculation of stresses associated with the debris-flow interior and granular-flow front could yield insight into the stresses causing bedrock incision.

For instance, following Iverson (1997), fluid shear forces in the fine-grained fluid interior of debris flows can be approximated as:

$$\tau_f \approx \nu_f \mu \frac{\partial u}{\partial z}, \qquad (2)$$

where ν_f is volumetric fluids concentration, μ is fluid viscosity, and $\partial u/\partial z$ is the shear strain rate. For muddy water, Iverson and Denlinger (2001) and Iverson and Vallance (2001) proposed viscosities of ~0.1 Pa/s.

At coarse-grained flow fronts, peak static normal solid stresses (σ_s) can be approximated using a Mohr-Coulomb expression for effective normal stress:

$$\sigma_s = (\nu_s \rho_p - \nu_f \rho_f) g h \cos(\theta) - p, \qquad (3)$$

where ν_s is volumetric solids concentration, ρ_p is particle density, ρ_f is fluid density, h is flow depth measured normal to the boundary, θ is slope angle, and p is the nonequilibrium component of intergranular fluid pressure (Iverson and Vallance, 2001). Experiments reported by Major and Iverson (1999) indicate that surge heads can have negligible fluid pressures, so perhaps fluid pressure can be omitted from equation 3 when characterizing the granular snout.

Inertial solid stresses arise from particle collisions that result in fluctuations about the mean flow trajectory, a property often termed *granular temperature* (Ogawa, 1978) by analogy to the theory of ideal gas. Some authors (e.g., Iverson and Vallance, 2001) also use the term *collisional* to describe this stress, emphasizing its origin from inter-particle collision. Bagnold (1954) idealized these flow conditions as two planes of spheres sliding over each other under neutrally buoyant conditions and proposed that stresses generated by collision of these layers were proportional to the square of the velocity gradient across them because both the frequency of collisions and the change in momentum per collision were proportional to this gradient. Reductions in either the frequency or momentum change per collision by fluid damping or inelastic collisions would tend to reduce this dependency below quadratic. Kinetic theory (Jenkins and Savage, 1983; Haff, 1983; Campbell, 1990) and laboratory experiments (e.g., Bagnold, 1954; Savage and McKeown, 1983; Savage and Sayed, 1984; Craig et al., 1986; Craig et al., 1987; Capart et al., 2000) validated Bagnold's hypothesis that normal stress resulting from the sum of these fluctuating inertial particle impacts (σ_i) is:

$$\sigma_i = a_i \cos\alpha_i \lambda f(\lambda) \rho_p D_p^2 \left(\frac{\partial u}{\partial z}\right), \qquad (4)$$

where a_i is a constant, α_i is an angle determined by collision conditions, λ is linear grain concentration, $f(\lambda)$ is a function of linear concentration, D_p is particle diameter, and u is velocity. In Bagnold's experiments, a_i was 0.04, cos α_i was ~1, and $f(\lambda) = \lambda$. Iverson (1997) replaced the linear concentration factors λ in equation 4 with a volumetric solids concentration ν_s, so that this equation is approximately:

$$\sigma_i \approx \nu_s \rho_p D_p^2 \left(\frac{\partial u}{\partial z}\right)^2. \qquad (5)$$

By dimensional analysis, Campbell (1990) and Hsiau and Jang (1998) argued that granular temperature is proportional to the last two factors of expression 5 under nonconducting conditions.

Ratios of stresses provide nondimensional numbers that are rough guides to the predominance of a particular stress. For instance, Savage and Hutter (1989) used the ratio of solid inertial normal stress to total normal stress to characterize the importance of particle collisions on total stress. On the basis of experiments, they proposed that a value of 0.1 represented a crude boundary above which particle collisions dominate over Coulomb frictional interactions. Iverson (1997) and Iverson and Vallance (2001) used a ratio of inertial to static normal stress to characterize the same transition, calling it a Savage number. As part of our field studies, we attempt to estimate the relative significance of viscous and inertial forces. To do so we follow Savage and Hutter's (1989) definition and propose to estimate the ratio of inertial normal stress to total normal stress as:

$$N_{SH} = \frac{\nu_s \rho_p D_p^2 \left(\frac{\partial u}{\partial z}\right)^2}{\nu_s \rho_p D_p^2 \left(\frac{\partial u}{\partial z}\right)^2 + (\nu_s \rho_p - \nu_f \rho_f) g h \cos(\theta) - p} \approx \frac{D_p^2 \left(\frac{u_s}{h}\right)^2}{D_p^2 \left(\frac{u_s}{h}\right)^2 + g h \cos(\theta)}, \qquad (6)$$

with the assumptions that fluid content and pressure are negligible (at the coarse-grained snout of the debris flow), and that the strain rate ($\partial u/\partial z$) can be approximated as the surface velocity u_s, divided by the total flow depth h. We also report the Savage number using Iverson and Vallance's (2001) definition (N_{Sav}). A ratio of inertial to viscous stress leads to the Bagnold number:

$$N_{Bag} = \frac{\nu_s \rho_p D_p^2 \frac{\partial u}{\partial z}}{\nu_f \mu} \approx \frac{\nu_s \rho_p D_p^2 \frac{u_s}{h}}{\nu_f \mu}. \qquad (7)$$

Values >200 for N_{Bag} are thought to indicate the predominance of inertial stresses (e.g., Iverson, 1997).

Limitations to Calculating Solid Stresses

There are substantial challenges to the field application of equations 5, 6, and 7 to calculate the stresses that debris flows exert on valley floors. These include uncertainty in the exponent on shear strain rate, the difficulty of estimating shear strain rate, and the ambiguity of the relevant grain size to use for a given distribution.

Experimental data suggest that the dependence on shear strain rate may be less than quadratic under some conditions. For instance, at non-neutrally buoyant conditions, gravity causes adjustments in solid volume fractions with depth to balance the normal component of body force (McTigue, 1982) and reduces the exponent slightly below 2 if conduction of granular temperature occurs (Hsiau and Jang, 1998; Hsiau and Shieh, 1999). Hanes and Inman (1985) found that the addition of fluid also reduced the exponent for $\partial u/\partial z$ to as low as 1.5. They attributed this reduction to viscous damping of impacts by pore fluids that might reduce either the frequency of impacts or the momentum transfer per impact below linear dependencies on $\partial u/\partial z$. Lun and Savage (1986) predict a similar reduction for inelastic collisions.

Uncertainties in the exponent for shear strain rate are currently outweighed by the practical difficulty of estimating shear strain rate from field measurements. Field data can be used to approximate shear strain rate as the surface velocity estimate u_s divided by flow depth h (e.g., Savage and Hutter, 1989; Iverson, 1997; Iverson and Denlinger, 2001; Iverson and Vallance, 2001). However, experiments on flowing granular masses (Hirano and Iwamoto, 1981; Nakashima, 1986; Davies, 1990; Cuogiang et al., 1993; Taylor and Hunt, 1993; Azanza et al., 1997; Capart et al., 2000; Longo and Lamberti, 2000) indicate that linear approximations of shear strain rate can underestimate near-boundary shear-strain-rate values by up to an order of magnitude. This is particularly true of rough boundaries, which can increase inertial normal stresses by large factors over linear approximations (e.g., Hanes and Inman, 1985). Calculation of equation 5 from field measurements using u_s

and h likely underestimates boundary stresses from inertial impacts.

There is no general agreement in the literature about how to calculate inertial normal stress in equation 5 when there is a grain size distribution. This is important because the choice of representative grain diameter can alter inertial stress estimates from equation 5 by orders of magnitude. For instance, Iverson (1997) and Iverson and Denlinger (2001) use particles between 0.001 and 0.2 m diameter to characterize distributions in natural debris flows, leading to solid inertial stresses that are more than an order of magnitude smaller than static solid stresses for their field examples. According to Bagnold (1954), the grain size enters the problem as the scale for the mass of the particle of interest, the scale for the vertical spacing between shear layers, the scale for the number of particles per bed area, and the scale for the number of collisions per unit of time. Hence, D enters as both the scale for the mass of grains and the concentration of grains in the flow. In grain mixtures, it is not obvious that one grain size would serve as the scale for both of these factors, though one might argue that there is an effective grain size whose mass and concentration are what matter for a bulk stress calculation.

Field measurements of grain size at the coarse fronts of active debris flows (Gol'din and Lyubashevskiy, 1966; Okuda et al., 1977; Okuda et al., 1978; Okuda et al., 1979; Watanabe and Ikeya, 1981; Suwa et al., 1984; Suwa et al., 1993) and debris-flow deposits (Suwa and Okuda, 1980; Suwa and Okuda, 1983) indicate that coarse-fraction mean and median grain sizes may vary from 0.1 m to several meters in diameter. Stock (2003) modeled theoretical elastic impact stresses from a coarse-grain-size distribution and concluded that a small percentile of the coarsest fraction (e.g., D_{88}–D_{96}) resulted in most of the inertial normal stress. On the basis of this calculation and preceding observations, we hypothesize that median grain sizes from gravel and coarser particles characterize the inertial normal stress that causes bedrock lowering under coarse-grained flow fronts. We use D_e (effective diameter) to represent this crude characterization of coarse particle size. In Table 1 we calculate solid static normal stresses by assuming near dry conditions in the surge head, with a volumetric solid fraction of 0.6, a particle density of 2650 kg/m^3, and locally measured slopes and peak-flow depths normal to the bed. We calculate fluid shear stresses for interior flow portions by assuming a viscosity of 0.1 Pa/s for muddy water (Iverson and Denlinger, 2001); these values are presented indirectly as the Bagnold number (N_{Bag}) in Table 2, where particle diameter is given a range between 0.001 and 0.2 m, suggested by reference to Iverson (1997).

To calculate inertial normal stresses in equation 5, we assume a volumetric solid fraction of 0.6, a particle density of 2650 kg/m^3, and approximate shear strain rate as u_s/h, where velocities are back-calculated using this equation and peak flow depths are locally measured. We use median boulder diameters observed in debris-flow terminal lobes to represent particle size in equation 5, although we are aware that such estimates have great uncertainty because of the ambiguity in characterizing particle diameter.

Rock Weathering

We hypothesize that duration of physical and chemical bedrock weathering between debris-flow events increases progressively upvalley, because the number of contributing debris-flow sources (i.e., link magnitude) decreases. As a result, bedrock valley floors should be increasingly weathered above each tributary that produces a mobile debris flow. Debris flows that do not make it to the main stem will not influence this pattern. For instance, field observations indicate that debris flows tend to deposit where they encounter junction angles greater than ~60°–70° (Ikeya, 1981; Benda and Cundy, 1990; Ishikawa, 1999). Benda and Dunne (1997) used the term *trigger hollows* to refer to hollows without sharp junction angles whose landslides generated debris flows that transited most of the network to deposit at low gradients on main-stem valleys. Slope and weathering characteristics should covary most strongly with the distribution of these trigger hollows.

While mapping the locations of trigger hollows, we estimated rock weathering using a type N Schmidt hammer along valleys recently scoured to bedrock by debris flows. Rebound (or R) values from this instrument represent a measure of bedrock elastic properties within a sampling length on the order of decimeters or less (e.g., Selby, 1980). Rebound values are influenced by rock matrix conditions as well as larger-scale fractures. We collected rock weathering data only in reaches with extensive bedrock exposure (typically >75% of valley length) because we did not wish to bias sampling toward steep, persistently exposed reaches whose harder

TABLE 2. ESTIMATES OF NONDIMENSIONAL NUMBERS CALCULATED FROM FIELD OBSERVATIONS

Location	Site	Lithology	Erosion features	N_{SH}	N_{Sav}	N_{Bag} D_p = 0.001 m	N_{Bag} D_p = 0.2 m	$N_{erosion}$
Oregon	ODF#535	"	abrasion, folia, grooves, block-plucking	5.9E–02	6.3E–02	1.9E+06	9.7E+03	2.7E+01
Coast Range	ODF#733	"	"	4.0E–03	4.0E–03	5.0E+05	2.5E+03	5.6E-01
	Sullivan 1	"	"	1.1E–02	1.1E–02	6.9E+05	3.5E+03	1.3E+01
	RockCr.#1	med. ss	abrasion, block-plucking	3.4E–02	3.5E–02	2.2E+06	1.1E+04	3.0E+01
	#2	(Yamhill Fm.)	soil scour	6.7E–02	7.2E–02	2.8E+06	1.4E+04	1.3E+02
	#3	"	"	1.1E–02	1.1E–02	1.6E+06	7.9E+03	5.8E+01
	#4	"	abrasion, block-plucking	2.1E–02	2.2E–02	1.9E+06	9.7E+03	9.6E+01
	#5	"	"	6.4E–03	6.4E–03	1.2E+06	6.2E+03	4.4E+01
	#6	"	soil scour	5.8E–02	6.1E–02	3.0E+06	1.5E+04	2.8E+02
	#7	"	"	8.8E–03	8.9E–03	1.4E+06	6.8E+03	5.9E+01
	#8		"	1.4E–02	1.4E–02	1.5E+06	7.4E+03	8.1E+01
S. Cruz Mtns., CA	Hiway9	arkose	"	1.8E–02	1.8E–02	1.6E+06	8.0E+03	2.0E+00
Wasatch, UT	Joe's#1	quartzite	"	7.4E–03	7.4E–03	9.1E+05	4.5E+03	2.2E+01
	#2	"	"	2.1E–02	2.1E–02	1.3E+06	6.3E+03	6.5E+01
San Gabriels, CA	Bear Cr.	granodiorite	"	1.4E–01	1.7E–01	3.2E+06	1.6E+04	-
		"	"	7.4E–02	8.0E–02	2.3E+06	1.1E+04	-

Notes: N_{SH} estimated using equation 6; N_{Say} estimated as the ratio of inertial to static normal solid stresses; N_{Bag} estimated using equation 7 with a viscosity of 0.1 Pa/s and a volumetric solids fraction of 0.6; $N_{erosion}$ calculated using equation16 with a bulking rate of 1m^3/m, initial failure volume of 100 m^3, tensile strength of 10^6 Pa, E_{eff} of 10^9 Pa, and D_f of 0.5 m.

rock (e.g., cliff-forming sandstones) might be more resistant to erosion. Starting with the landslide headscarp (link magnitude 0), we stratified sampling sites by link magnitude (including non-trigger hollows), sampling at two locations in each link of the runout path equidistant from the link ends. At each of the two sites within the link, we took 100 *R* values using a random walk over a bedrock valley floor area ~10 m long by 2–4 m wide. We adjusted the exact locations of these sites within each link so that we sampled sites of the same lithology down the runout track (i.e., we sampled sandstones, not a mixture of sandstones and siltstones or mudstones). We characterized the weakest remaining portion of the bedrock using the 25th percentile of Schmidt hammer *R* values; other low percentiles yield a similar pattern. On an opportunistic basis, we measured planform dimensions of 50 fracture spacings at some sites by random walk sampling. These approximate the dimensions of fractured blocks that could be entrained by debris flows.

RESULTS

Bedrock Erosion by Debris Flows and Attendant Bulk Stresses

Field observations along recent debris-flow runouts in Washington, Oregon, California, and Utah record bedrock lowering by four main mechanisms: impact loading, plucking, abrasion, and grooving (Fig. 7). These four lowering mechanisms are present to varying degrees along the runouts of debris flows in Figure 4 and Table 1, many of them extending to the point at which deposition occurs at terminal levees. However, lowering from abrasion and from grooving during sustained sliding contact are small multiples of the bedrock grain size (millimeter scale), ~1–2 orders of magnitude less than individual block removal (centimeter to decimeter scale) recorded in Table 1 and Figure 7. Patchy block removal is the most effective lowering mechanism at these sites, occurring along decimeter-scale regional fracture or joint sets. For instance, Figure 7A illustrates a fresh fracture surface that resulted from the impact removal of a large decimeter-sized block of quartzite by a debris flow at Joe's Canyon, Utah. Similar gaps are visible in Figure 7B. At the same cross section, fresh fractures (Fig. 7C) indicate point-loading by objects entrained in the flow and resulting tensile failures.

In the Oregon Coast Range sites, the plucking of weathering folia appears to be the largest component of bedrock lowering because of their large dimensions and common occurrence. For instance, a large ledge in Figure 7D records the removal of a platelike rock fragment 7 mm thick and many centimeters in lateral extent. We measured 9805 of these fractured plates of rock, or folia, along Sullivan Creek tributaries and found a median thickness of 7 mm, a mean thickness of 9 mm, and typical plan-view dimensions of tens of centimeters (see Table 1 for local values). We measured similar values along two Marlow Creek runouts, with median thicknesses of 4–7.5 mm for 1721 samples. Curiously, post-scour weathering features like the tent in Figure 7D are rare and appear to form soon after the debris-flow passage. We have observed no new physical weathering features subsequent to our installation of 363 erosion pins in Oregon bedrock valley bottoms several months after debris flows in the winter of 1996–1997 (Stock et al., 2005).

A more distributed form of lowering is recorded by abrasion, forming faint lineations by removing weakly bound particles (e.g., sand grains) from the weathered bedrock matrix (Table 1; e.g., Fig. 7D). Moss preserved in the lee of a ledge in Figure 7D indicates that abrasion here was patchy and less than several multiples of the bedrock sand-grain diameter, or several millimeters. Local removal of weathering patinas, shown in Figure 7B, records similar millimeter-scale lowering by this process.

Evidence for sustained, large-particle indentation (grooves) is rare. For instance, Figure 7E records the sustained sliding indentation of an object that resulted in a narrow 1–3-mm-deep groove. Table 3 lists the dimensions of all grooves that we could find along ~700 m of a Sullivan Creek tributary during an exhaustive 1 m hand-level survey. It illustrates that grooves occupy <1% of the scoured area.

Table 1 records estimates of surge-head velocity and path-length averaged bulking values. Path-length averaged values of bulking range from ~0.01 to 10 m^3/m for debris flows in Oregon (e.g., Benda, 1990; Table 1). These averaged values of bulking vary greatly, some between adjacent, seemingly similar valleys (e.g., Marlow 1 and 4), so that initial landslide volumes may vary from 1% to nearly 100% of final deposit volume. These values can be calculated from Table 1 by subtracting the product of the bulking rate and runout length from the total fan volume. Figure 8 illustrates the lack of systematic variation in surge-head depth along individual runouts. These flows grow longer, rather than deeper, as they entrain material.

At sites where we estimated surge flow depth, valley slope, and velocity (Table 1), estimates of static solid (equation 3) and inertial normal (equation 5) stresses in the granular flow front are listed. At these sites we observed evidence for bedrock lowering by inertial impacts. Even if fluid is present in large amounts in the surge head, our estimates for large D_e would necessarily result in ratios of solid inertial normal stresses to viscous shear stresses (equation 7) that are larger than 10^4 for all sites, suggesting the predominance of solid stresses. Bulk solid static normal stresses are close to values calculated using similar assumptions by Benda (1985) for debris flows in the Oregon Coast Range and are far below megapascal values required to break intact rock (e.g., Table 1 *in* Goodman, 1980). Yet solid inertial normal stresses are 1–2 orders of magnitude smaller than solid static values, although there is evidence for the failure of rock by point loads (Fig. 7). In Table 2, corresponding Savage-Hutter numbers (equation 6) range from order 10^{-3} to 10^{-1}. Savage numbers (e.g., Iverson, 1997) are not substantially different because of the minor change in the denominator of equation 6 with these particular estimates of inertial stress.

A Systematic Slope Pattern with Trigger Hollows

We found a tendency for main-stem slope to decrease abruptly downvalley from trigger hollow tributary junctions (e.g., Fig. 9). Addition of a tributary with a non-trigger hollow (one that joins at angles greater than 70° to the main-stem valley) has a negligible effect on valley slope at these sites. Debris-flow valley slopes from Scotsburg (Fig. 10) illustrate that over similar drainage areas the slope of valleys with more than one debris-flow source decreases, whereas those with only one source have approximately constant slopes. Both plots are consistent with the hypothesis that slope is adjusted to the number of upvalley, mobile debris-flow sources.

There is significant scatter along these profiles, largely because of rock bedding and fractures. We have observed that a few widely spaced fractures, or thick beds, may lead to local steep slopes, creating valley slope fluctuations between junctions with trigger hollows (e.g., Fig. 10). Locally strong forcing of slope by variations in fracture density or bedding thickness creates irregularities in most debris-flow runout long-profiles (e.g., Fig. 5). It appears that large changes in link magnitude are required to create resolvably different slopes where lithology and fracture spacing variations occur.

A Systematic Weathering Pattern with Trigger Hollows

The proportion of weak, weathered bedrock remaining on the valley floor *after* a debris flow has passed increases as link magnitude

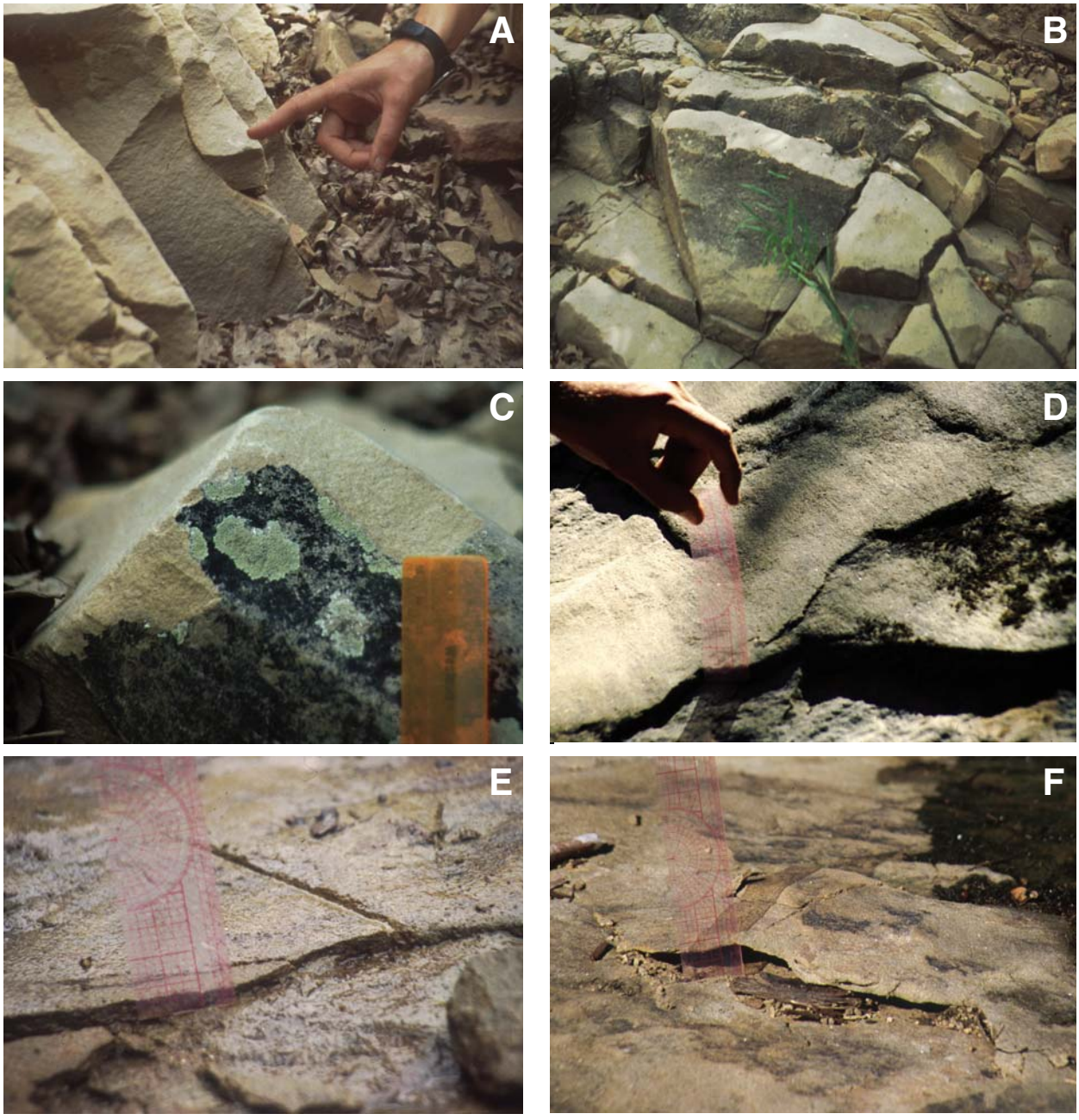

Figure 7. Evidence for bedrock lowering by debris flows; upvalley at top of all photos. See Table 1 for approximate estimation of bulk stresses at selected sites. (A) Impact loading, resulting in removal of decimeter-sized block of quartzite at Joe's Canyon, Utah. (B) Plucking and abrasion of weathering patina from jointed bed of Joe's Canyon. (C) Tensile failure of quartzite in Joe's Canyon debris flow. (D) Removal of sandstone grains (~0.5–1 mm in diameter) on Sullivan Creek tributary by abrasion. Moss in the lee of the smaller ledge indicates abrasion of less than several millimeters. Ledge at bottom of photo corresponds to removal of fractured slab 7 mm thick. (E) Rare 1–3-mm-deep groove on Sullivan Creek tributary runout, indicating sustained sliding contact of particle for at least 190 mm along the bed. Adjacent 9-mm-deep ledge indicates removal of a wide rock tablet following groove formation. See Table 3 for all groove dimensions. (F) Post-event weathering feature ("tent") along Sul1, observed ~1 mo. after debris flow. Subsequent monitoring indicated that these features were no longer forming. Note the removal of the dark weathering patina by abrasion during the debris flow.

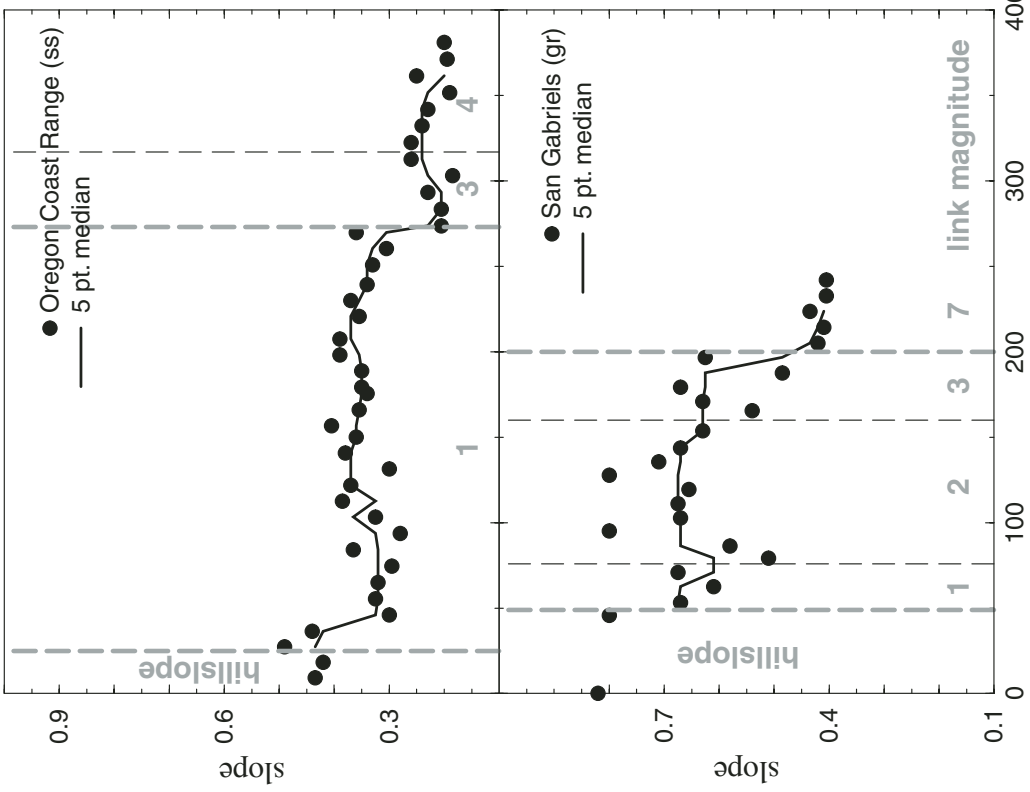

Figure 9. Evidence from field surveys for a step reduction in reach slope as trigger link magnitude increases (heavy vertical dashed lines). Data from debris-flow runouts over rock with unusually homogeneous fracture density and bedding in the Oregon Coast Range (Silver Creek) and the San Gabriel Mountains (Redbox). Note that non-trigger hollows (light dashed lines) do not substantially influence reach slope in these examples; gr—granite; ss—sandstone.

TABLE 3. DIMENSIONS OF GROOVES CUT IN EOCENE TYEE FORMATION BY DEBRIS FLOWS

Slope	Depth (mm)	Width (mm)	Length (mm)
0.20	0.7–0.8	3.5–4.0	36
0.20	2.4–3.7	1.4–1.8	101
0.08	0.4–1.0	2.0–3.0	196
0.25	4–5	1.5	2200
0.25	5–8	1.5–2	2160
0.25	3–7	1	800
1.34	2–3	1	105

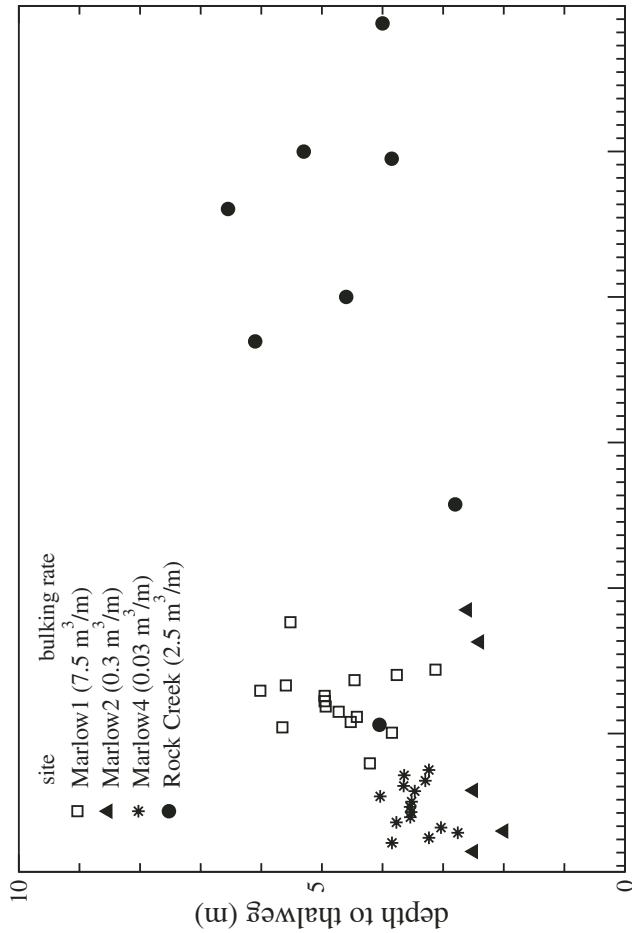

Figure 8. Field data from Oregon, illustrating no consistent increase in debris-flow depth with runout distance for some of the flows listed in Table 1. Depths are maximum vertical distance from thalweg to trim line. Bulking rates for each event are shown in parentheses.

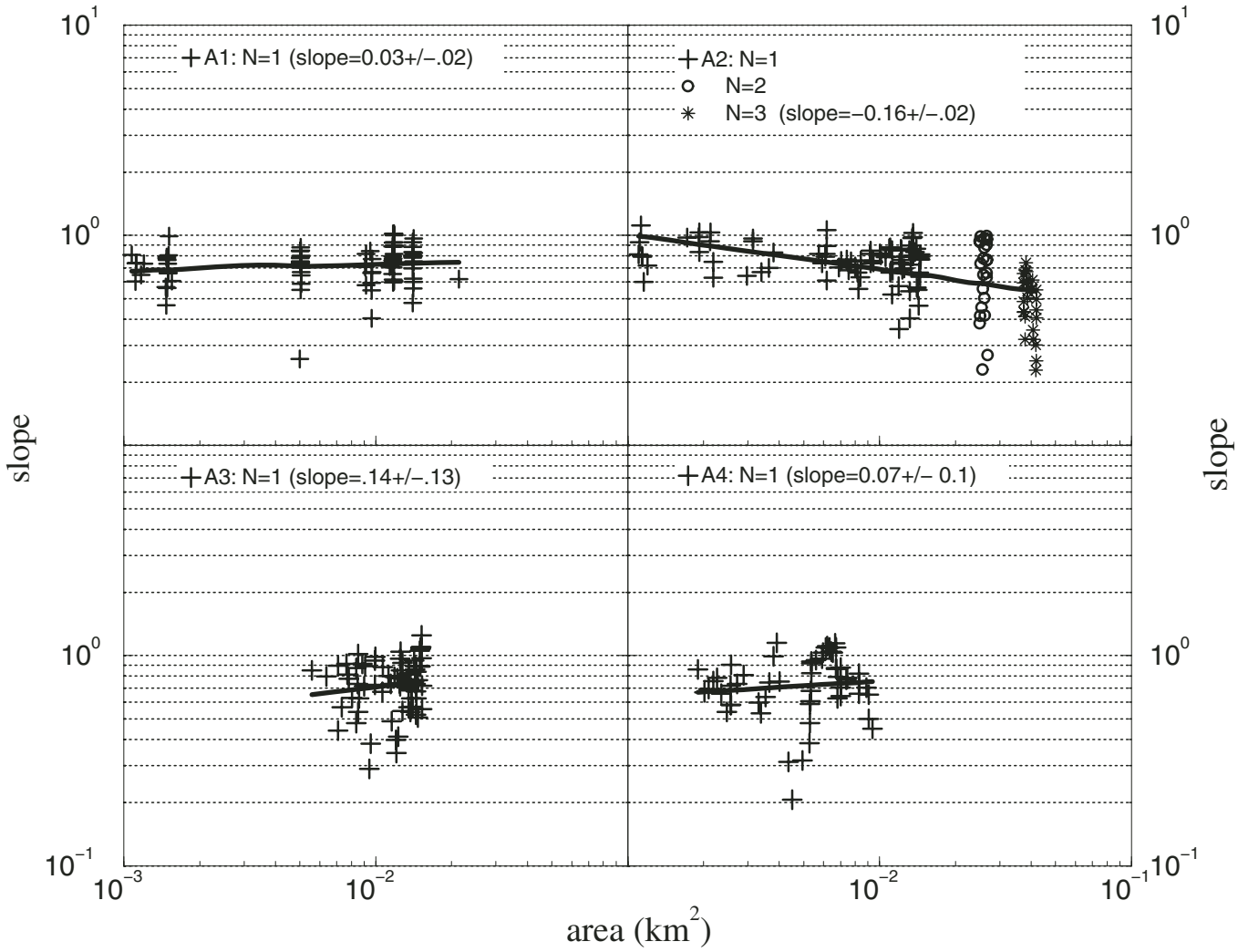

Figure 10. Evidence from Scotsburg laser altimetry (Fig. 4B) for the influence of link magnitude N on valley slope. Slope and standard error of least squares regression shown in parentheses. Slopes of valleys with only one debris-flow source (A1, A3, and A4) do not change at a statistically significant level, indicating that these links have linear long-profiles. By contrast, valleys that gain more than one debris-flow source (A2) have reductions in slope.

decreases (Figs. 11, 12). This field evidence of systematic increases in rock weathering with network position indicates that weathering is a potential adjustment to changes in debris-flow scouring frequency through the network. Changes in valley floor rock strength are not resolvable at trigger link magnitudes >5–7 for the basins we studied; it is possible that frequent or intense downvalley debris-flow scour obscures weathering. Reaches with low link magnitude tend to correspond to the upper left part of the area-slope plot where slope does not vary much with drainage area (e.g., Fig. 13). An exception to the trend of downvalley increasing rock strength occurs at a fan head at the Pescadero site. This weathered bedrock valley floor is consistent with long periods of burial in depositional fan sites.

CONCEPTUAL FRAMEWORK FOR A DEBRIS-FLOW INCISION LAW

Network Properties

Field observations and data from the preceding section lead to a view of debris-flow incision summarized in Figure 3. Mobile debris flows initiate at landslides clustered near basin heads, gain mass as they translate, and erode at rates that depend on the length of the granular flow front and the velocity with which the coarse grains hit the bed. Network structure matters because it controls the relative frequency of events at a given reach. For instance, if the valley network is to approach steady-state lowering, the downvalley increase in scouring frequency ought to be balanced by some combination of abrupt reductions in rock weathering or slope reductions that lower particle impact velocities. In the following paragraphs we hypothesize crude topographic parameterizations for (1) long-term event frequency, (2) bulking rate as it influences granular flow front length L, (3) flow depth h, and (4) streamwise flow velocity u_s. We use these hypotheses to illustrate how network variations in these properties change valley long-profiles. The parameterizations are by no means unique, so they also illustrate our current lack of knowledge about debris-flow properties through networks.

We parameterize the long-term frequency of debris flows along the main stem as the ratio of upvalley trigger hollows to their average landslide failure interval, N_t/t_r. Trigger hollows that generate mobile debris flows tend to cluster

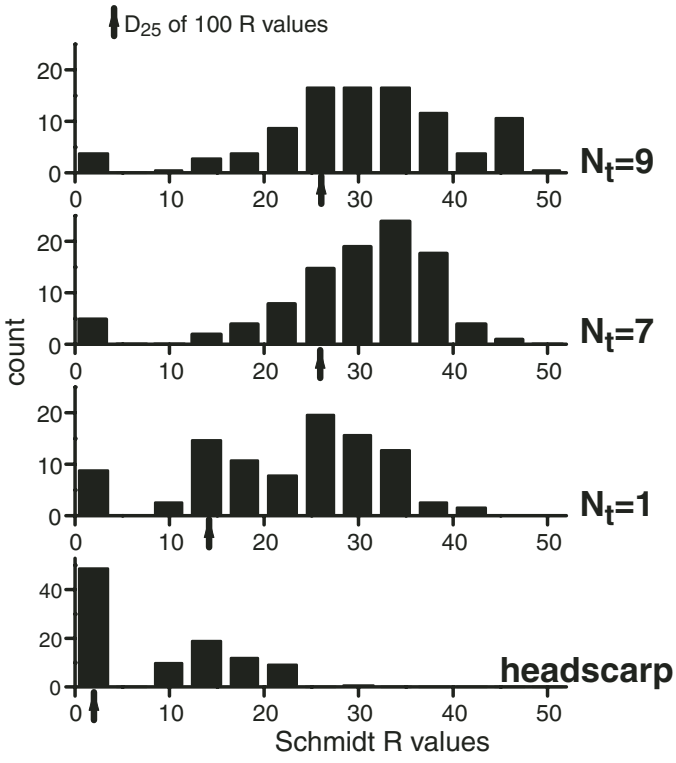

Figure 11. Distribution of Schmidt hammer rebound (R) values with trigger link magnitude (N_t) for the same sandstone on the Sul1 tributary to Sullivan Creek. R values are a proxy for rock tensile strength. See text for sampling details. Note the systematic increase in the proportion by area of weak, weathered rock toward landslide headscarp, as characterized by the 25th percentile of *R* values.

at the head of basins, resulting in a nonlinear gain in trigger hollow sources along the main stem near the basin headwaters (e.g., Fig. 14). We assume that each trigger hollow generates equally mobile debris flows and that debris flows generated elsewhere are not mobile along the main stem.

We reason that an initial flow length, characterized as the ratio of flow volume to the product of flow width and height, increases with progressive material entrainment at longer runout distance, higher bulking rates, and higher volumetric solids fractions. It is likely that path-length averaged bulking rates (e.g., Table 1) conceal rate variations within the network owing to event sequencing and network structure. In particular, bulking rates along the main stem are likely to increase rapidly in the lower basin where the flow encounters deposits from both hillslopes and nonmobile debris-flow tributaries. To capture the effect of rapidly increasing bulking rates in the lower basin, we hypothesize that bulking rate is an exponential function of drainage area, normalized by the total drainage area. This exponential factor modifies the initial ratio as:

$$L(x) = \frac{k_1 v_0}{w(x) \cdot h(x)} e^{a_1 \left(\frac{A(x)}{A_{total}} \right)}, \quad (8)$$

where k_1 determines what fraction of the initial landslide length will convert to a granular front, v_0 is initial landslide volume, w is debris-flow width, h is surge head height, A is drainage area, A_{total} is the total drainage area of the debris-flow basin, and a_1 is a dimensionless bulking exponent. The first factor is a ratio that represents the average flow front length (i.e., initial volume divided by width and depth), modified by a fraction k_1. The second factor expresses spatial variation in L along the main-stem long-profile owing to bulking rate variations. The normalization by total drainage area is necessary to yield observed L values from several meters to several tens of meters at terminal levee deposits. Additionally, if the initial debris-flow granular front is of the order of 1 m, a_1 cannot be larger than ~4, or terminal snout lengths will exceed those commonly observed at deposits in the field sites of Table 1. Given that bulking rates appear to vary substantially between basins, there is reason to expect that a_1 will also vary. Large variations in bulking rates between adjacent basins in Table 1 could reflect variations in rock type, producing coarse debris, or time elapsed since a previous event.

Curiously, most entrained material is added to the length of the debris flow, as surge head depth does not appear to vary greatly downstream in available field studies (e.g., Fig. 8; Davies, 1990; Benda, 1990; Mizuyama et al., 1993). Depth appears at most a weak function of drainage area:

$$h = k_2 A^{a_2}, \quad (9)$$

where a_2 is a positive number <<1 and k_2 has dimensions of $1/(2a_2)$ so that h has units of length.

In contrast to water velocities in river networks, the streamwise velocities of debris-flow fronts have a tendency to decrease as slope declines through the network. This would also tend to reduce the velocities of particles hitting the valley floor, reducing rock lowering rates. Figure 15 illustrates power law fits to velocities from debris flows on Mount Yakedake, Japan, and from the Oregon Coast Range. Little generality can be inferred from such fits other than that they represent a strong central tendency for faster debris flows on steeper slopes. We parameterize this tendency using a power law expression for slope with a variable exponent:

$$u_s = k_3 S^{a_3}, \quad (10)$$

where k_3 has units of velocity and may vary greatly in time and space. We suspect that the exponent a_3 varies at least between 0.2 and 1.2, perhaps with network geometry (i.e., junction angles). Representing velocity with this substitution assumes that individual basins have a characteristic exponent a_3, a proposition that has yet to be demonstrated. In the absence of a mechanistic understanding of velocity variation through these networks, this crude parameterization captures some spatial variation of velocity owing to slope, as noted by previous workers (e.g., Gol'din and Lyubashevskiy, 1966; Okuda et al., 1980b; Suwa and Yamakoshi, 2000).

Stress Properties

Field evidence suggests that rock lowering occurs primarily by impact removal of fracture-bounded blocks during inertial stresses, not grooving or abrasion from application of sliding, static normal stresses. Yet bulk estimates

of both stresses using equations 3 and 5 (e.g., Benda, 1985; Table 1) are of the order of tens of kilopascals at the most, 10–1000 times less than tensile strengths of many intact rocks (e.g., Table 1 *in* Goodman, 1980). It is likely that debris flows at Table 1 sites lowered bedrock either by point-load failures during excursions from bulk inertial stresses or by plucking of weathered joint blocks. Evidence for patchy lowering may reflect episodic impact of particles large enough to cause bedrock failure or the preexisting distribution of loosened joint blocks. For instance, large particles that collided with the bed have caused point loads from 0.1 to 10 MPa in some debris flows (Okuda et al., 1977; Sabo Publicity Center, 1988) sufficient to break many intact rocks (e.g., Goodman, 1980). We hypothesize that peak stresses from point-load impacts become proportionally larger as bulk inertial normal stress increases, so that a dimensionless constant K_0 relates the two values. Then a rate law that characterizes debris-flow incision rate into bedrock would be proportional to expression 5 with a coefficient of K_0. Insofar as granular temperature is proportional to expression 5, this hypothesis is equivalent to stating that lowering rates scale with the fluctuating component of particle velocity.

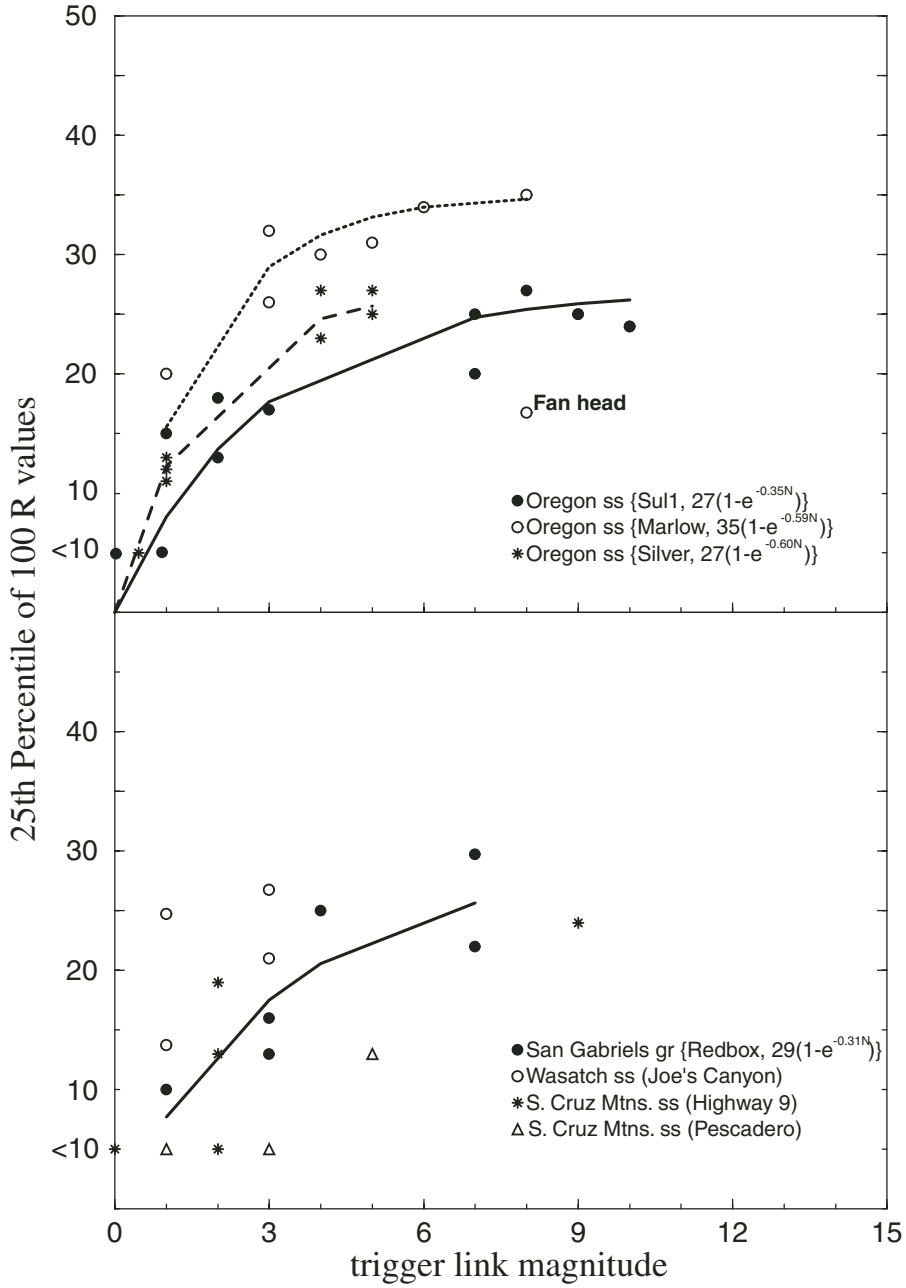

Figure 12. Summary of field evidence for systematic increase in weak bedrock with link magnitude, approaching landslide headscarps in granite (gr) and sandstone (ss). Note the reduced R value at the fan head for Marlow Creek. R values <10 are indistinguishable with the Schmidt hammer and are offset for clarity. Curves are fits to the expression in parentheses, an empirical equation that allows R values to approach the maximum measured value at large trigger link magnitude N_t. Wasatch and Santa Cruz Mountain sites have insufficient data to fit. See Table 1 for site details.

To date, the treatment of inertial normal stresses has ignored the effect of slope on equation 4. Debris flows may occur on exceedingly steep slopes (e.g., >70°), so some modification of expression 5 seems necessary to account for a likely reduction in particle impact frequency approaching free-fall conditions. We hypothesize that at slopes well above 100%, the along-slope hop-length for a particle, or layer of particles, might tend to increase as 1/cosθ. This reduces the frequency of collisions in equation 5 by a cosine factor:

$$\sigma_i \approx \cos(\theta) v_s \rho_p D_p^2 \left(\frac{\partial u}{\partial z}\right)^2, \qquad (11)$$

so that impact frequency along the cliff face approaches zero at free fall.

Rock Properties

Rock discontinuity spacing and intact rock properties such as tensile strength ought to influence transient lowering rates from failure during particle impact. By analogy to the Griffith crack theory (cf. Jaeger and Cook, 1976), we hypothesize that rock resistance to crack growth during indentation or unloading is characterized by the work done opening tensile failures: T_0^2/E_{eff}, where T_0 is tensile strength and E_{eff} is effective elastic modulus. Experimental and field data (cf. Fig. 6.5 *in* Lo and Hefny, 2001) indicate that denser fracture spacing reduces E_{eff}, leading to deeper indentation.

We hypothesize that transient lowering rates increase with fracture density because denser discontinuities (1) reduce the modulus of deformation E_{eff}, leading to deeper indentation and larger chip formation for a given impact; and (2) increase the probability of an additional free surface toward which impact-related tensile failures can migrate, resulting in higher probabilities of block plucking over chipping. Because both effects depend upon the size of the indentor relative to the fractured block,

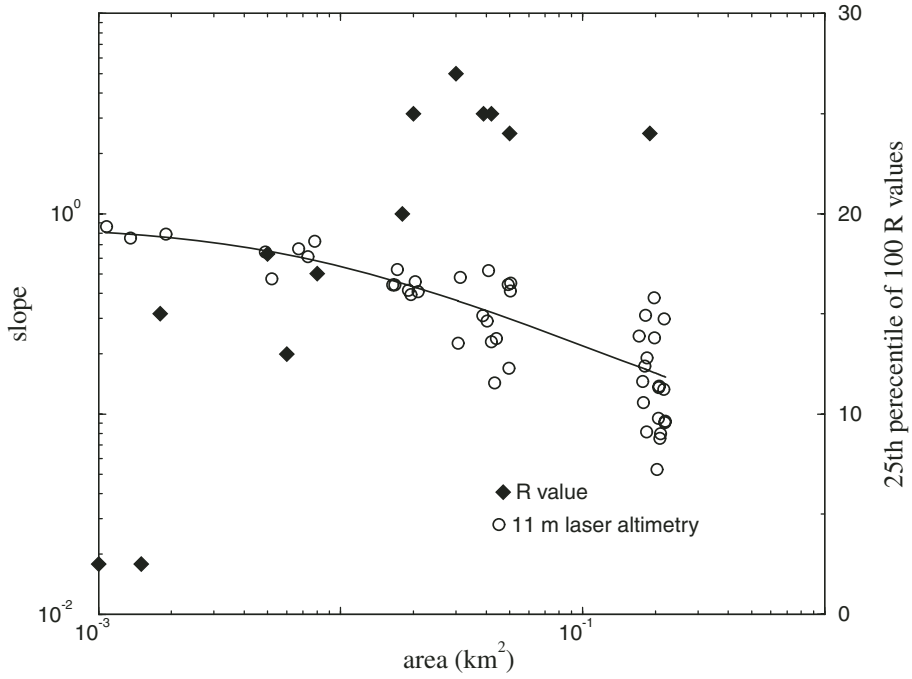

Figure 13. R values from Figure 12, plotted in relation to slope and drainage area for Sul1, illustrating common occurrence of an observable rock weathering (reduced R values) with reduced curvature of area-slope data. Slopes are averaged along-valley over 11 m intervals, because this interval represents the coarsest averaging possible before curve fit changes.

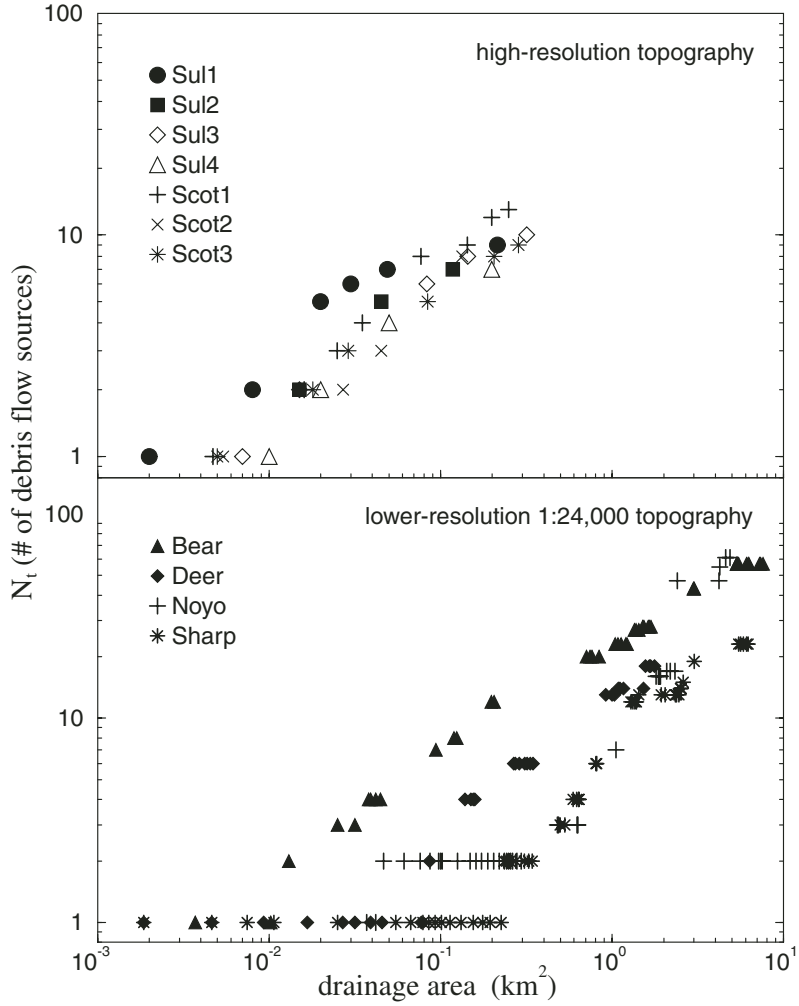

Figure 14. Plots of the rate at which mainstem valleys gain throughgoing debris-flow sources (trigger hollows, N_t) with drainage area. Trigger hollows in the upper plot are identified using high-resolution topography from Figure 4. Bottom plot is a comparatively crude (note the range of drainage area for a single hollow) estimate of trigger hollow numbers from 1:24,000-scale contour maps of debris-flow basins previously investigated in Stock and Dietrich (2003). In both plots the number of debris-flow sources is rarely characterized by a power law without nonrandom residuals.

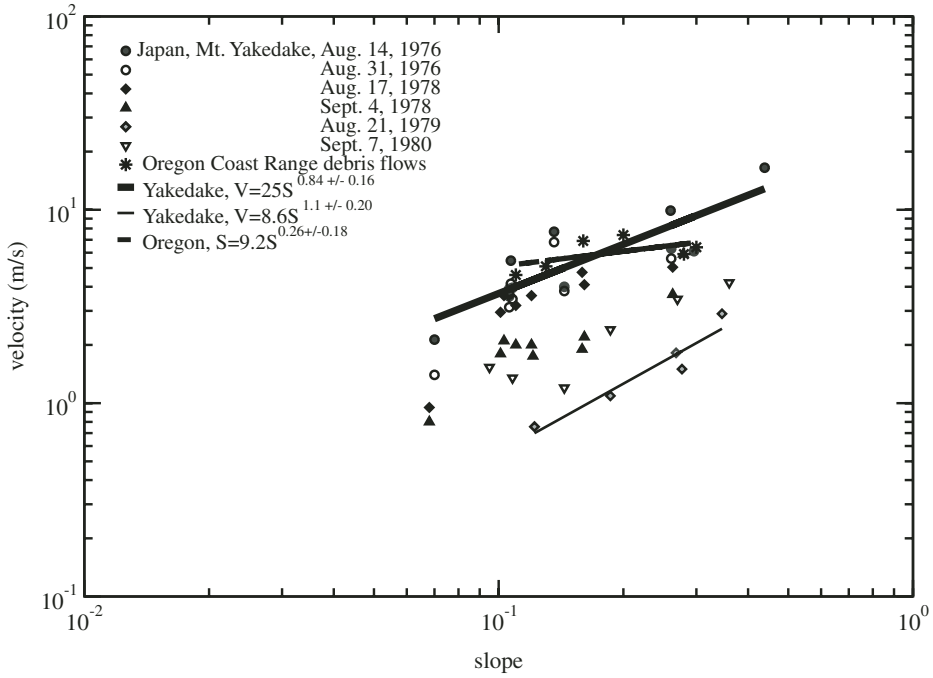

Figure 15. Field data from Kamikamihori Valley on Mount Yakedake, Japan (Okuda et al., 1977, 1979, 1980a, 1981) and Rock Creek in Oregon, illustrating the tendency for debris flows to slow down as slope decreases. Note that this tendency exists despite the large variation in velocity for different debris flows in the same valley. Japanese data are from video camera estimates; Oregon data are back-calculated using equation 1 (in text).

the effect of fracture spacing on lowering rate ought to be scaled by the indentor diameter, D_p. We propose $D_f/(D_f + D_p)$ as a nondimensional measure of indentor volume, so that as fracture spacing D_f is increasingly larger than particle diameter, the ratio tends toward unity for massive rocks (characterized solely by tensile strength and deformation modulus). This results in a rapid decline in lowering rates as discontinuity spacing exceeds the dimensions of the impactors.

Sklar and Dietrich (2001) demonstrated an inverse squared dependence of rock lowering rates on tensile strength in a bed-load abrasion flume, and field measurements of bedrock lowering rate are also consistent with this relation (Stock et al., 2005). Experiments by Hsu and Dietrich (2004) also showed that erosion by grain flows for several different material strengths collapsed onto a line when normalized by the tensile strength squared. Rock excavation rates from tunnel boring machines and rock cutting trenchers increase rapidly with denser fracture spacing (Franklin et al., 1971; Fowell and Smith, 1976; Aleman, 1981; Karpuz et al., 1990; Pettifer and Fookes, 1994; Thuro, 1997; Vervoort and De Wit, 1997; Deketh et al., 1998; Thuro and Plinninger, 1999). These machines are analogous to debris flows in the sense that rock removal is accomplished by energetic impacts and point loading.

On the basis of field observations and literature described previously, we hypothesize that a measure of rock resistance to lowering by particle impacts is:

$$\frac{T_0}{E_{\text{eff}}}\left(\frac{D_f}{D_f + D_p}\right), \tag{12}$$

where T_0 is tensile strength measured by the Brazil strength test (e.g., Vutukuri et al., 1974; Sklar and Dietrich, 2001), D_f is a measure of reach-scale fracture density (e.g., median fracture spacing D_f of random walk count; Table 1), and D_p is particle diameter (e.g., the median grain size D_e at bouldery fronts of debris flows).

Recurrence intervals between debris flows can be decades to thousands of years for entire basins with many debris-flow sources (e.g., Orme, 1990; Yoshida et al., 1997; Harris and McDermid, 1998; Cerling et al., 1999; Eaton et al., 2003). Long-term recurrence intervals at landslide initiation sites are correspondingly greater, approaching many thousands of years near the tips of networks (e.g., Benda and Dunne, 1987; Reneau and Dietrich, 1991; Eaton et al., 2003). The variation in event frequency through the network appears to result in a pattern of increasingly weathered rock toward network tips, balancing the reduction in event frequency.

For instance, Figures 11–13 indicate that systematic reductions in rock strength may occur above junctions with trigger hollows at link magnitudes 1–8. These reductions are consistent with deeper rock weathering as the time interval between debris flows increases. We hypothesize that episodic debris flows erode more deeply into weathered bedrock carapaces so that the product of event frequency with event lowering approaches a constant value. If so, depth and intensity of rock weathering would be inversely proportional to the number of upvalley debris-flow sources (trigger links) up to a certain value above which incremental changes in weathering are not measurable (e.g., ~5–8 in Fig. 12). We hypothesize that tensile strength T_0 declines toward valley heads owing to longer exposure between events as:

$$T_0(N_t) = T_0\left(1 - e^{-c_2 N_t}\right), N_t \geq 1, \tag{13}$$

where c_2 is a constant (e.g., Fig. 12) that characterizes the rate of decline. Equation 13 is an attempt to generalize the network pattern of R values in Figure 12; its utility elsewhere is unknown.

HYPOTHESIS FOR A DEBRIS-FLOW EROSION LAW

Event Expression

On the basis of field observations of localized rock damage from impacts, we hypothesize that debris-flow lowering rates increase with bulk inertial normal stresses. If the cumulative force of the particle impacts that cause erosion scales linearly with bulk inertial normal stresses approximated by expression 11 with a generalized exponent w, transient debris-flow incision rates are proportional to the integral of inertial normal stress along the eroding portion of a flow of unit width and the frequency of flows f and are inversely proportional to rock resistance. One expression of this is:

$$-\frac{\partial z}{\partial t} = \frac{K_0 K_1}{\frac{T_0^2}{E_{\text{eff}}}\left(\frac{D_f}{D_f + D_e}\right)} \cdot f \cdot$$

$$L\left[\cos(\theta)\nu_s \rho_p D_e^2 \left(\frac{\partial u}{\partial z}\right)^w\right]^n, \tag{14}$$

where K_0 is a dimensionless proportionality constant relating bulk inertial normal stresses

to higher excursions of inertial normal stress, K_1 is a proportionality constant between rock resistance and incision rate, L is the length of the flow front with large grains (e.g., Fig. 2) capable of eroding high tensile strength rock, n is an exponent of unknown value, and D_e is the median boulder diameter at a surge head. K_1 has dimensions that vary with w and n so that the right side of expression 14 will have units of erosion rate (e.g., K_1 is dimensionless if w is 2 and n is 1). Although we set $n = 1$ in the following analyses, we include it to account for the possibility that erosion is nonlinear with inertial normal stress. The frequency term f is N_t/t_r (i.e. the number of trigger hollows divided by the typical hollow landslide recurrence interval).

We approximate $\partial u/\partial z$ as u_s/h where u_s is the streamwise velocity, as measured by runup or other field techniques, and h is flow depth at the coarse front as estimated by trimlines or terminal deposits. We treat the exponent w as a variable, which likely varies from ~1 to 2 (Hanes and Inman, 1985). A rate law whose variables could be estimated for debris flows from field and lab measurements is:

$$-\frac{\partial z}{\partial t} = \frac{K_0 K_1}{\frac{T_0^2}{E_{\text{eff}}}\left(\frac{D_f}{D_f + D_e}\right)} \cdot f \cdot L\left[\cos(\theta)\nu_s \rho_p D_e^2 \left(\frac{u_s}{h}\right)^w\right]^n. \quad (15)$$

Equation 15 predicts that fast, shallow, frequent flows with big rocks and long, granular snouts are most erosive. It is consistent with numerous wear experiments, showing that wear rates are the sum of many micromechanical failures from single-particle impacts whose intensity is a function of particle density, diameter, velocity, and impact angle (e.g., Finnie, 1960; Sheldon and Finnie, 1966; Neilson and Gilchrist, 1968; Sheldon and Kanhere, 1972; Evans et al., 1978; Hockey et al., 1978; Wiederhorn and Lawn, 1979; Routbort et al., 1980; Wiederhorn and Hockey, 1983; Lhymn and Wapner, 1987; Meng and Ludema, 1995; Gahr, 1987; Goretta et al., 1999; Stack et al., 1999).

A ratio of bulk, solid, inertial normal stresses integrated along a path of unit width to rock resistance illustrates a nondimensional number that scales with the erosion rate predicted by equation 15:

$$N_{\text{erosion}} = \frac{\cos(\theta)\nu_s \rho_p D_e^2 \left(\frac{u_s}{h}\right)^2 \left(\left(\frac{v_f - v_0}{v_0}\right)\frac{x}{x_f} + \frac{v_f}{v_0}\right)}{\frac{T_0^2}{E_{\text{eff}}}\left(\frac{D_f}{D_f + D_e}\right)}. \quad (16)$$

Here, v_0 and v_f are initial failure volume and final runout volume, x is runout length, and x_f is total runout length. This ratio characterizes lowering under idealized, dry, fully elastic conditions where w is 2. The last factor in the numerator contains terms that represent a bulking rate nondimensionalized by initial failure volume and multiplied by a runout distance x. This factor is meant to represent the growth of the length of the granular flow front with bulking rate. The last term in it is a quotient of the final to initial failure volume and allows nonzero erosion numbers if there is no bulking up. Note that equation 16 is independent of flow volume and is intended to characterize variations in stresses along a runout path that leads to a characteristic long-profile shape. At valleys with evidence for bedrock lowering by debris flows, typical values for N_{erosion} are of the order 10^0–10^2 (Table 2). These estimates of N_{erosion} covary with inertial normal stress and runout length because we assumed constant values for v_0 (100 m^3), bulking (1 m^3/m), rock fracture spacing (0.5 m), tensile strength (10^6 Pa), and elastic modulus (10^9 Pa), *in lieu of* field measurements for these at *all* sites. The full range of values at which rock lowering occurs remains to be explored.

Geomorphic Transport Law

Several of the factors in equation 15 have spatial and area dependencies such that erosion according to this expression could lead to drainage area and slope relationships and overall long-profile shape that could be compared with measurements (e.g., Stock and Dietrich, 2003). If expressions 8–10 and 12 and 13 are substituted into expression 15, an expression for debris-flow incision is:

$$-\frac{\partial z}{\partial t} = \frac{K_0 K_1}{\frac{T_0^2}{E_{\text{eff}}}\left(1 - e^{-c_2 N_t}\right)^2 \left(\frac{D_f}{D_f + D_e}\right)} \cdot \frac{N_t}{t_r} \cdot \frac{k_b v_0}{w(x) \cdot k_2 A^{a_2}} e^{a_1\left(\frac{A(x)}{A_{\text{total}}}\right)} \cdot \left[\cos(\theta)\nu_s \rho_p D_e^2 \left(\frac{k_3 S^{a_3}}{k_2 A^{a_2}}\right)^w\right]^n. \quad (17)$$

For the sake of a simple illustration, suppose that rock properties, bulking coefficient k_b, and debris-flow width, depth, grain size, and solids concentration do not vary along a debris-flow runout. If their product is a constant K_2, equation 17 becomes:

$$-\frac{\partial z}{\partial t} = K_3 \cdot \frac{1}{\left(1 - e^{-c_2 N_t}\right)^2} \cdot \frac{N_t}{t_r} \cdot e^{a_1\left(\frac{A(x)}{A_{\text{total}}}\right)} \cdot \cos^n(\theta) S^{a_3 w n}, \quad (18)$$

where K_3 represents the product of K_0, K_1, and K_2. The second factor on the right side of equation 18 represents variation in rock weathering with link magnitude; the third factor, the frequency of events; the fourth factor, the rate of granular-flow-front growth owing to bulking; and the last factor, a slope dependency on inertial normal stress. If granular temperature is a function of slope, a similar reasoning could lead to such a slope dependency. In this form, equation 18 encapsulates variables that may lead to a rate law and distinct topographic signature for debris-flow incision, including (1) a weathering dependency in the denominator that becomes unimportant at large trigger link magnitude N_t (e.g., 10); (2) a dependence on the rate at which debris-flow sources accumulate within the network (N_t); (3) a dependence on landslide recurrence interval (t_r); (4) a bulking expression representing the length of the erosive, coarse-grained flow front; and (5) a slope dependency that arises from conversion of streamwise velocity to surface-normal particle impacts, and the resulting damage mechanics ($S^{a_3 w n}$), counterbalanced by a decrease in impact frequency approaching free-fall [$\cos^n(\theta)$].

Long-Profile Evolution Modeling

To illustrate the debris-flow incision expression, we take modern debris-flow valley long-profiles and parameterize them in terms of equation 18. We erode these valleys using the observed valley long-profile and distribution of trigger hollows downvalley as initial conditions, using equation 18 for 10 Ma, after which time the long-profiles do not change shape. At the Table 1 sites, this steady-state time scale represents erosion through about three relief envelopes (as suggested by Howard, 1994). The model is one dimensional, so to account for the network properties of the field sites, we map trigger hollow locations with distance along the main stem (Table 4). We vary the constant K_3 in equation 18 so that the steady-state incision rate at the bottom of the long-profile matches estimated boundary lowering rates shown in Table 4. We then compare the evolved long-profile to the initial condition to evaluate how well equation 18 recreated observed debris-flow long-profiles.

We used detailed long-profiles from recently scoured debris-flow valleys at Sullivan and Scotsburg (Fig. 5), and coarser 1:24,000-scale

TABLE 4. SITE PARAMETERS FOR LONG-PROFILE EVOLUTION WITH EQUATION 18, ASSUMING $c_2 = 0.35$, $n = 1$, AND $w = 2$

Location	Site	Lithology	Erosion rate (m/yr)	A_c (m^2)	A_{total} (m^2)	$A = cx^a$ (m^2)	Trigger link magnitude changes along valley long-profiles (N_t<*x*-coordinate of junction>N_{t+1}<*x*-coordinate of next downvalley junction>…)
Oregon Coast Range	Sullivan Creek#1	sandstone	0.0001	2000	220190	$4.07x^{1.73}$	**1**<32>**2**<104>**5**<185>**6**<215>**7**<339>**9**
	#2	"	"	3000	146672	$143x^{1.11}$	**1**<84>**2**<114>**4**
	#3	"	"	7000	328534	$5.45x^{1.66}$	**1**<111>**2**<154>**7**<372>**8**<397>**9**<536>**15**
	#4	"	"	10000	203178	$15.4x^{1.46}$	**1**<142>**2**<212>**4**<313>**8**<514>**9**
	Scottsburg#1	"	0.0002	4700	269492	$17.9x^{1.45}$	**1**<131>**2**<189>**3**<248>**4**<351>**8**<579>**9**<726>**12**<850>**13**
	#2	"	"	2000	145472	$4.78x^{1.62}$	**1**<148>**2**<277>**3**<387>**8**
	#3	"	"	5000	281132	$4.10x^{1.73}$	**1**<122>**2**<162>**3**<193>**5**<404>**8**<609>**9**
Oregon Cascades	Sharp's Creek	metavolcanics	0.0001	2000	6192905	$83.7x^{1.32}$	**1**<431>**2**<722>**3**<845>**4**<1103>**6**<1184>**12**<1460>**13**<2123>**14**<2282>**15**<2348>**19**<2444>**31**
California Coast Range	Noyo River	greywacke	0.0004†	36000	4877795	$15.6x^{1.54}$	**1**<144>**2**<1062>**3**<1233>**7**<1341>**16**<1623>**17**<1995>**47**<2229>**55**<2385>**61**
	Deer Creek	sandstone	0.0003‡	2000	1768349	$9.62x^{1.60}$	**1**<270>**2**<372>**4**<555>**6**<912>**13**<1152>**14**<1599>**18**
San Gabriels	Bear River	granodiorite	0.001	3000	7573028	$3.23x^{1.78}$	**1**<93>**2**<153>3<231>**4**<354>**7**<411>**8**<471>**12**<609>**20**<992>**23**<1382>**27**<1640>**29**<2102>**43**<2492>**57**

Note: A_c is the drainage area at the valley head, A_{total} is the drainage area at the end of the debris-flow zone, and *L* is length along valley; see field sites section of text for additional lowering rate references.
†Projection of marine terrace rock uplift rates from Merritts and Vincent (1989) inland.
‡Estimated from sediment yield (Brown, 1973) and cosmogenic radionuclide analysis of sediment (Perg et al., 2000).

contoured debris-flow long-profiles from four sites in the western United States (Table 4) that we explored in Stock and Dietrich (2003). We convert these data to 200 equally spaced elevation points by applying a spline to each input long-profile. We calculate slope with a 2-cell forward difference, and we approximate drainage area A in terms of long-profile distance x using the relation $A = A_c + cx^a$ (Table 4). A_c represents a threshold drainage area above which data tend to follow a power relation cx^a and is not related to valley head. We substitute this expression into expression 8 to calculate the increase in granular flow front L as the flow bulks up along the runout. We characterize N_t along each long-profile by mapping tributaries with junction angles <70° against main-stem runout distance x. The last column of Table 4 lists the value of N_t, the main-stem x-coordinate of the tributary junction, and the next downvalley N_t value. The use of equation 18 assumes that debris-flow width and depth are approximately constant, which is consistent with data in Table 1 and Figure 8. We use c_2 weathering values derived from Sul1 (Fig. 12). For the sake of simplicity, we assume that $n = 1$ and $w = 2$ in equation 18. We apply equation 18 and maintain the initial slope of the last point on the profile at each time step to simulate equilibrium lowering using finite-difference methods outlined in Stock and Montgomery (1999). The constant slope boundary condition forces the model long-profile to approach the downvalley slope of the initial long-profile. For this reason, parameter values are highly sensitive to lower boundary slope values. Variations in rock properties or transients at these endpoints would have a disproportionately large effect on resulting parameter values.

Figure 16 illustrates how variations in weathering (c_2), bulking (a_1), velocity (a_3), and stress (n) exponents influence steady-state long-profiles of Sul3. These parameter variations are referenced to a long-profile whose parameters ($a_1 = 1.0$; $a_3 = 0.9$) closely approximate the existing one using a field value of $c_2 = 0.35$ from Sul1 and assuming that $n = 1$ and $w = 2$. Kinks in the long-profiles correspond to changes in the number of mobile debris-flow sources N_t. Increases in the magnitude of the weathering exponent reflect increasingly less weathered rock (see

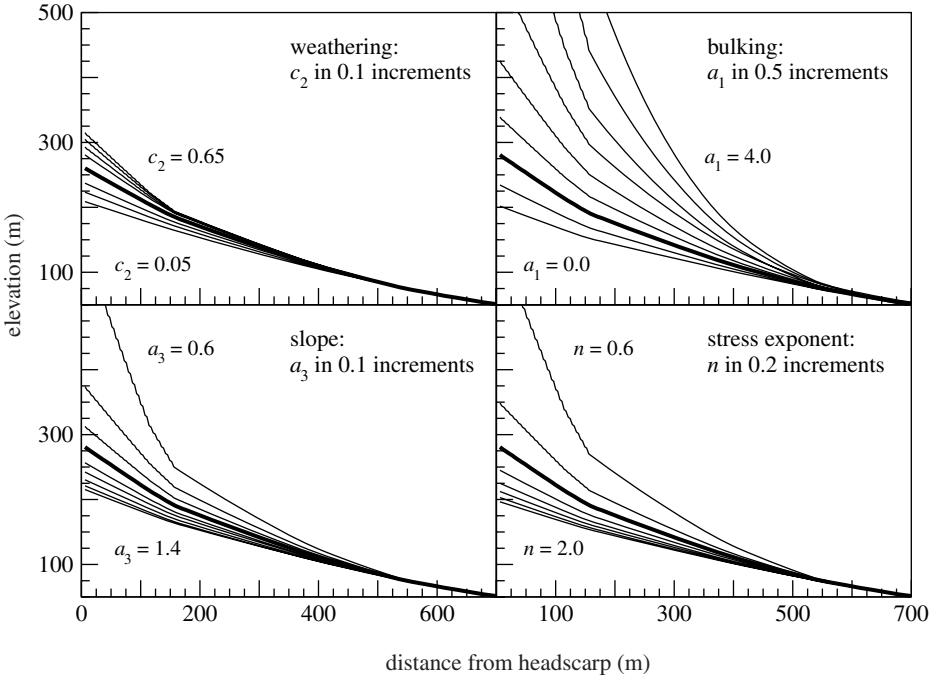

Figure 16. Different steady-state long-profiles after the application of a debris-flow incision law (equation 18) to Sul3 valley (Fig. 4A). Each panel illustrates long-profiles perturbed from a bold line that represents a model long-profile whose bulking ($a_1 = 1.0$) and velocity ($a_3 = 0.9$) exponent values reproduce Sul3, given measured weathering values ($c_2 = 0.35$), and assuming a stress exponent of $n = 1$. Kinks in the long-profiles correspond to changes in the number of debris-flow sources, N_t. Increases in the magnitude of weathering and bulking exponents (top panels) lead to increased steady-state relief, whereas increases in exponents on slope (bottom panels) lead to reduced relief. See text for further explanation.

Fig. 12) and result in increasingly large relief as the long-profile steepens to maintain the boundary-lowering rate. Increases in the bulking exponent increase the gradient in granular flow front L along the profile, leading to increasing curvature and relief as increases in L are balanced by reductions in slope to match the boundary-lowering rate. The bulking exponent may depend on the boulder content of the colluvium in the valley fill, which in turn would depend on rock type and incision rate. By contrast, increases in exponents that are applied to slope (a_3 and n) reduce the gradient in this factor along the profile, resulting in reduced steady-state relief.

Figure 17 illustrates the range of bulking and velocity exponents that best reproduce existing valley long-profiles and reliefs at Table 4 sites. Within this field, velocity exponents below ~0.3 poorly reproduce most initial long-profiles. Velocity exponents above 2.0 are also unlikely because they require bulking exponents that are unreasonably large (e.g., >4). However, long-profile simulations summarized in Figure 17 indicate that no single combination of the parameters in equation 18 explains the long-profile shape of all of the original valleys. For instance, for a velocity exponent of 0.9, a value allowed by all of the long-profiles, bulking exponents vary from ~0.0 to 2.1 (Fig. 17). It is not clear whether this variation reflects mechanistic differences expressed by the model, variations in the long-profiles from lithology or transient conditions, or deficiencies in the model.

Figure 18 illustrates that equation 18 maintains several key initial long-profile features, including abrupt slope reductions at tributary junctions with large increases in trigger hollows (e.g., Sul3 between N_t = 2 and 7) and reduced curvature in the uppermost long-profile. The resulting long-profiles also maintain curved area-slope data (Fig. 6) characteristic of debris-flow valleys. This is a consistency test that indicates that parameters in expression 18 can be arranged to yield reasonable long-profiles. It is in no way a validation of the model. We will need to have independent means of extracting velocity and bulking exponents before a more rigorous test of equation 18 is possible.

However, equation 18 is an improvement over fluvial models based on power law regressions through area-slope data of Figure 6. These models systematically underpredict valley relief in Figure 18 because they do not capture slope-area curvature with rapid changes in slope at downvalley drainage areas. Nor do fluvial models with constant curvature capture the tendency for linear slopes at low drainage areas that characterize most debris-flow valleys (Stock and Dietrich, 2003).

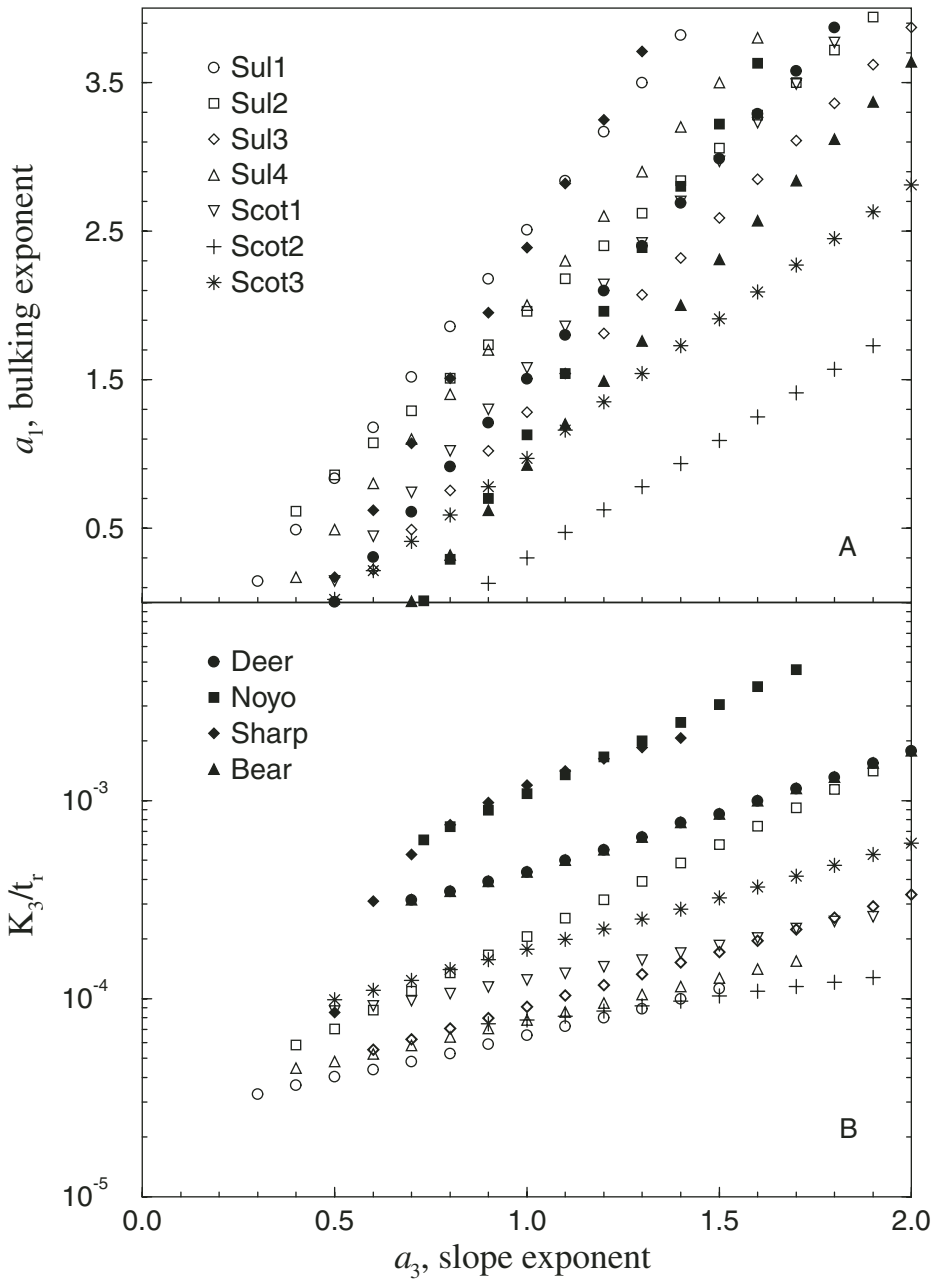

Figure 17. (A) Plot of bulking exponent versus velocity exponent from equation 18. These combinations resulted in model long-profiles that closely reproduced existing valley long-profiles (Fig. 4) after they were evolved to steady state using the debris-flow incision law. Bulking exponents must be limited to values that produce terminal granular flow fronts less than ~50 m for a conservative initiation length of 1 m (i.e., a_1 less than ~4). Most of these combinations yield a shape and relief that reasonably match the real long-profile, and we have no independent evidence to prefer one combination over another, save the observation that velocity exponents do not appear to exceed ~1.3 (Fig. 14). (B) Plot of constant K_3/t_r required in equation 18 to reproduce estimated boundary lowering rates for each long-profile (see Table 4). Landslide recurrence interval is set to 2 ka for all long-profiles for purposes of comparison, although much of the variation in K_3 between sites may be due to unknown variations of t_r.

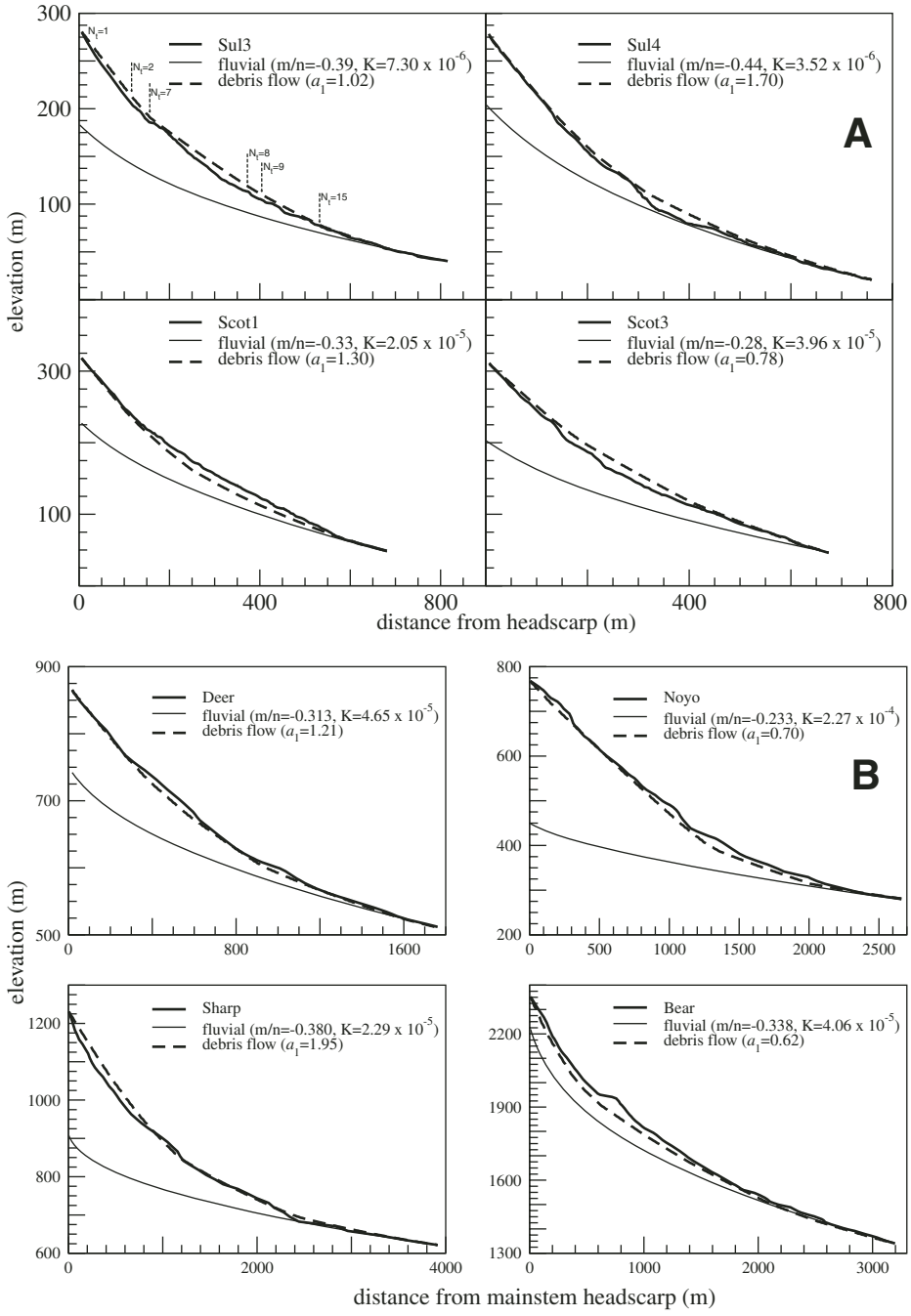

Figure 18. Comparison of selected long-profiles from (A) laser altimetry (see Fig. 4), and (B) contour maps, to steady-state fluvial and debris-flow incision models. Sul3 panel (A) illustrates plotting of N_t data from Table 4 on long-profile. Dashed fluvial long-profiles calculated using m/n value from Figure 6, assuming that n = 1 (e.g., Stock and Montgomery, 1999). Debris-flow incision models evolved using equation 18 with Table 3 parameters, with a_3 = 0.9, the lowest possible velocity exponent that results in fits to all of the valleys in Figure 18A. Fluvial models underestimate relief because they do not capture rapid increases in slope in the curved area-slope data of Figure 6, and they show profile curvature in their upper reaches that is not present in real long-profiles. Debris-flow models capture abrupt slope changes at tributary junctions and linear upper sections of long-profiles, but variations in long-profile shape and lower boundary conditions of each long-profile lead to substantial variation in best-fit bulking exponent a_1. Note that the large bump in the Bear long-profile is roadcast.

DISCUSSION

Approximations for debris-flow incision rate in equations 17 and 18 have factors that are fundamentally different from those found in stream power laws. For instance, we propose that the planform arrangement of tributaries matters to the long-profile of the channel because tributary junction angles can limit the passage of erosive debris flows. This network structure also influences the degree of weathering of the bedrock in the upper valley network and the bulking rate of debris flows (k_1), which in turn influence the length of the erosive snout of the debris flow. The stress driving impact removal of rock is an inertial stress associated with granular collisions, with a strong dependency on streamwise bulk flow velocity. The grain size dependency of this process in equation 18 is carried in a coefficient. Finally, we expect the wear to decline on very steep slopes owing to reduced inertial normal stress as particle impact frequency declines.

Many geomorphically relevant debris-flow properties remain unquantified, and models of velocity, weathering, and bulking that are more mechanistic than those hypothesized and incorporated into equation 17 will be required to validate a debris-flow incision law. Flume studies are under way to verify that inertial normal stresses are the relevant stresses leading to bedrock erosion. Observations of granular flows in a small rotating-drum flume by Hsu and Dietrich (2004) are consistent with the use of inertial stresses as approximated by expression 5 to characterize bedrock lowering by impacting particles. The same experiments support the hypothesis that energetic impacts occur at the front of the flow, so that snout length L is the appropriate scaling length for erosive power. In the meantime, equation 18 expresses in crude form the features that are seen in the field (Figs. 9, 11–13) like abrupt slope and weathering reductions with the accumulation of debris-flow sources. Applied to existing long-profiles, the expression predicts equilibrium curved area-slope signatures (Fig. 6) as a result of slope reductions to compensate for increases in debris-flow frequency and bulking. It also reproduces the linear long-profiles of debris-flow valleys where weathering adjustments may predominate. The expression of these features is an improvement over stream power laws calibrated by regressing area-slope data with a power law. We suggest that a form of equation 18 should be applied to valleys above the scaling transition, as defined by the transition from log-log linear to curved data in area-slope plots (see Stock and Dietrich, 2003). However, it is possible to approximate each debris-flow cut long-profile with a stream power law so long as substantial variation in K, m, and n is allowed

among different valleys. These fits lack curved area-slope data, but they can approximate relief. Lague and Davy (2003) take this approach, and, although this simplified approach is practically useful, it lacks a basis in field observations or mechanics; hence it provides limited value in exploring process controls on topography.

The use of slope exponents $0.8 < n < 1.2$ in equation 18 results in equilibrium long-profiles that closely match all of the examples, if bulking exponents are varied. This variation may result from real variation in bulking rates (e.g., Table 1), from transients or lithologic variations, or from flawed parameterizations of velocity or bulking. If equation 18 is to be used to simulate long-profile evolution, slope and bulking exponents that lead to reasonable relief for given long-profiles should be used (e.g., values for Sul3 of $a_1 = 1$ and $a_3 = 0.9$). The present utility of equation 18 is its identification of some of the variables that can be reasoned to influence debris-flow incision rates. For instance, rock types that do not produce particles large enough to cause impact damage, or steep slopes that lead to greatly reduced impact frequencies, could lead to hillslopes without well-defined valley networks.

Equation 18 also predicts that debris-flow incision rates decrease proportionally as landslide recurrence interval grows, preserving relief. As a thought exercise to illustrate this hypothesis, suppose that the rivers of a steep landscape ceased lowering rapidly as crustal thickening and rock uplift end. Although debris flows continue to erode so long as landslides mobilize, an effectively constant elevation at debris-flow runout zones would result in a gradual reduction in valley slope that migrates upvalley toward landslide sources. In its wake, debris-flow incision rates decline because of lower inertial stresses from reduced flow velocities, leading to a reduction in adjacent hillslope gradients and soil flux. This further reduces debris-flow incision rate by reducing bulking rates, although landslide frequencies may not decline significantly until the reduced slope migrates to valley heads. Once this occurs, landslide failure requires increasingly extreme hydrologic events (e.g., Wieczorek et al., 2000), leading to significantly lowered debris-flow frequencies and lowering rates. This negative-feedback process, leading to longer and longer debris-flow recurrence intervals, may drastically reduce debris-flow incision rates.

In this thought experiment, valley relief above 0.03–0.10 slopes remains substantial for long periods of time as debris flows become increasingly infrequent with increasing landslide recurrence intervals. Such a scenario might explain the persistence of mountain ranges (e.g.,

TABLE A1. LIST OF SYMBOLS

a (–)	Exponent on drainage area as a power function of *x* (see long-profile evolution section)
a_1 (–)	Bulking exponent (8)
a_2 (–)	Depth exponent (9)
a_3 (–)	Velocity exponent (10)
a_j (–)	Constant from Bagnold (1954) (4)
A (m^2)	Drainage area (9)
A_c (m^2)	Threshold drainage area above which data on a graph of drainage area vs. downvalley distance are well approximated by power law (see long-profile evolution section)
A_{total} (m^2)	Drainage area at end of debris-flow long-profile (8)
c (–)	Constant in drainage area as a power function of *x*
c_2 (–)	Exponent characterizing the decline in weathering with increasing trigger link magnitude (13)
D_e (m)	Particle diameter characterizing the most effective size at eroding bedrock from a distribution, assumed to be the median diameter of boulders at flow front (14)
D_f (m)	Characteristic bedrock fracture spacing (e.g., median value from random walk) (12)
D_p (m)	Particle diameter, moment of a distribution (4)
E_{eff} (Pa)	Effective elastic modulus of fractured rock (12)
f (1/yr)	Long-term averaged frequency of debris flows at a point in the valley network (14)
g (m/s^2)	Gravitational constant (1)
h (m)	Debris-flow surge head depth (3)
k_1 (–)	Coefficient of proportionality in bulking expression (8)
k_2 ($f[a_2]$)	Proportionality constant between debris-flow depth and source area (9)
k_3 ($f[a_3]$)	Proportionality constant between streamwise debris-flow velocity and valley slope (10)
K_0 (–)	Constant of proportionality relating excursions in solid inertial normal stress to bulk solid inertial normal stress (14)
K_1 (f[n, w])	Proportionality constant between rock strength and erosion rate (14)
K_2 ($f[K_0, K_1$, numerous other parameters])	Constant characterizing any spatially invariant properties of debris-flow erosion (rock strength, debris-flow width and depth, grain size, solids concentration) (see Geomorphic Transport Law section)
K_3 ($f[K_0, K_1, K_2]$)	Product of K_0, K_1, and K_2 (18)
L (m)	Length of debris-flow granular front (8)
n (–)	Exponent characterizing the erosional efficiency of inertial normal stress (14)
N_{Bag} (–)	Bagnold number (ratio of solid inertial normal stress to fluid static stress) (7)
$N_{erosion}$ (–)	Ratio of path-integrated bulk inertial solid stresses to rock resistance (16)
N_{Sav} (–)	Savage number (ratio of solid inertial normal stress to static solid stress)
N_{SH} (–)	Savage-Hutter number (ratio of solid inertial normal stress to total solid stress) (6)
N_t (–)	Number of upvalley trigger hollows or mobile debris-flow sources (13)
p (Pa)	Nonequilibrium component of intergranular fluid pressure (3)
S (–)	Valley slope (10)
T_0 (Pa)	Rock tensile strength (12)
t_r (yr)	Long-term recurrence interval of landsliding at a hollow (17)
u (m/s)	Debris-flow velocity (4)
u_s (m/s)	Streamwise (along slope) velocity of debris flow (1)
v_0 (m^3)	Landslide volume (8)
v_f (m^3)	Debris-flow terminal deposit volume (16)
w (m)	Debris-flow width at surge head (8)
w (–)	Exponent relating shear strain rate to solid inertial normal stress; may vary with flow conditions (e.g., intensity of viscous damping or inelastic collisions) (14)
x (m)	Horizontal debris-flow runout distance, measured along main stem from landslide scarp (8)
x_f (m)	Total horizontal debris-flow runout distance, measured from landslide scarp (16)
α (–)	Velocity head coefficient from runup calculation (1)
α_j (–)	Friction angle from Bagnold (1954) (4)
$\partial u/\partial z$ (1/s)	Shear strain rate of debris flow (2)
$\partial z/\partial t$ (m/yr)	Bedrock surface lowering rate (13)
Δh (m)	Debris-line elevation difference from velocity runup (1)
λ (–)	Bagnold's (1954) linear solid concentration (4)
μ (Pa/s)	Viscosity of phase defined as fluid in debris flow (2)
ν_f (–)	Volumetric fluid concentration (2)
ν_s (–)	Volumetric solids concentration (3)
θ (–)	Valley slope angle (3)
ρ_p (kg/m^3)	Particle density (3)
ρ_f (kg/m^3)	Fluid density (2)
σ_i (Pa)	Solid normal inertial stress (4)
σ_s(Pa)	Solid normal static stress (3)
τ_f (Pa)	Fluid static shear stress (2)

Note: parentheses after symbols enclose units, – indicates dimensionless. Parentheses after definition indicate equation number where symbol was first used shown in parentheses.

Appalachians) long after rock uplift has ceased. In such places, there is evidence for long recurrence intervals (e.g., 1–10 ka) for debris flows (e.g., Woodruff, 1971; Williams and Guy, 1973; Bogucki, 1976; Pomeroy, 1980). Wieczorek et al. (2000) also found that rainfall intensity thresholds for some areas of Appalachia are much higher (and therefore less frequent) than in similarly steep slopes elsewhere. A frequency reduction in any event-driven erosion model would tend to preserve relief, but equation 18 predicts that relief in landscapes without active rock uplift is concentrated in valleys with only a few landslide sources, where slopes remain sufficiently steep to convey debris flows. In this sense, response time is strongly dependent on network structure. It provides an alternative to existing explanations, including those of Baldwin et al. (2003), who argued that the recruitment of coarse gravel armoring the bed from fluvial erosion may stop relief reduction, and Stephenson (1984), who argued for lithospheric flexure as a mechanism to preserve relief. This hypothetical example suggests that steepland topography may persist long after tectonism ceases if relief is dominated by debris-flow valleys, and landslide recurrence interval grows after rock uplift ceases.

CONCLUSION

Field observations at recent debris-flow runouts in temperate, soil-mantled steepland valleys with slopes above ~0.03–0.10 indicate recent bedrock lowering. We hypothesize that wear rate for a given rock type and weathered state is controlled by bulking rate, which influences the rate of growth of the granular front, and inertial stresses, which depend on grain size, velocity, depth, and slope. We hypothesize a debris-flow incision rate law that increases with flow length and solid inertial normal stress, and decreases with increasingly longer landslide recurrence intervals and harder rocks (characterized by tensile strength and fracture spacing). Forward modeling of this expression can reproduce equilibrium long-profiles similar to those from high-resolution field data, including the curved area-slope form that we propose as a signature for valleys cut by debris flows (Stock and Dietrich, 2003). This curvature results largely from the network structures' effect on long-term debris-flow frequency. The network structure influences the number of sources that produce debris flows that sweep down the channel (trigger hollows) and therefore the frequency of debris-flow scour. This influences the recurrence interval between wear events, which likely affects the degree of bedrock weathering along the valley floor. Much work remains to justify a debris-flow incision law, such as field and flume studies that explore relations between stress and rock-lowering rate, and improvements in topographic parameterizations for debris-flow properties like velocity and bulking rate. This effort is justified by the substantial portion of steep landscapes whose form depends on debris-flow incision, and the necessity of including details of this process that are not captured by area-slope power laws.

APPENDIX

See Table A1.

ACKNOWLEDGMENTS

We gratefully acknowledge field assistance from Douglas Allen, Dino Bellugi, Simon Cardinale, Mauro Cassidei, Tegan Churcher, Alex Geddes-Osborne, Taylor Perron, Cliff Riebe, Josh Roering, Joel Rowland, Kevin Schmidt, Adam Varat, and Elowyn Yager. Rick Giraud, Utah Geological Survey, kindly provided field notes and the location of several Utah landslides. Matt Anders, Alison Duvall, Geoff Phelps, Mark Reid, Kevin Schmidt, and Gerry Wieczorek generously provided helpful reviews. We especially thank Greg Tucker, Grant Meyer, and Frank Pazzaglia for their generous, thoughtful reviews. Figure 3 is by David Jones, U.S. Geological Survey. This work was supported by NASA SRTM NAG5-9629 and the U.S. Geological Survey's Mendenhall Post-Doctoral Program.

REFERENCES CITED

Aleman, V.P., 1981, A strata index for boom roadheaders: Tunnels and Tunneling, v. 1981, p. 52–55.

Armstrong, P.A., Ehlers, T.A., Chapman, D.S., Farley, K.A., and Kamp, P.J.J., 1999, Exhumation of the central Wasatch Mountains: Constraints from low-temperature thermochronometry: Eos (Transactions, American Geophysical Union), v. 80, p. F1034.

Azanza, E., Chevoir, F., and Moucheront, P., 1997, Experimental study of rapid granular flows in a two-dimensional channel, *in* Behringer, R.P., and Jenkins, J.T., eds., Powders and grains 97, Proceedings of the Third International Conference on Powders and Grains, Durham, North Carolina: Rotterdam, Balkema, p. 455–458.

Bagnold, R.A., 1954, Experiments on a gravity-free dispersion of large solid spheres in a Newtonian fluid under shear: Proceedings of the Royal Society of London, Ser. A, v. 225, p. 49–63.

Baldwin, J.A., Whipple, K.X, and Tucker, G.E., 2003, Implications of the shear stress river incision model for the timescale of postorogenic decay of topography: Journal of Geophysical Research, v. 108, ETG 7-1.

Benda, L., 1985, Delineation of channels susceptible to debris flows and debris floods, *in* Proceedings of the International Symposium on Erosion, Debris Flow and Disaster Prevention, Tsukaba, Japan: Tokyo, Toshindo, p. 195–202.

Benda, L., 1990, The influence of debris flows on channels and valley floors in the Oregon Coast Range, U.S.A.: Earth Surface Processes and Landforms, v. 15, p. 457–466.

Benda, L., and Cundy, T.W., 1990, Predicting deposition of debris flows in mountain channels: Canadian Geotechnical Journal, v. 27, p. 409–417.

Benda, L., and Dunne, T., 1987, Sediment routing by debris flow, *in* Beschta, R.L., Blinn, T., Grant, G.E., Swanson, F.J., and Ice, G.G., eds., Erosion and sedimentation in the Pacific Rim: Proceedings, International Association of Hydrological Sciences no. 165, p. 213–223.

Benda, L., and Dunne, T., 1997, Stochastic forcing of sediment supply to channel networks from landsliding and debris flows: Water Resources Research, v. 33, p. 2849–2863, doi: 10.1029/97WR02388.

Blythe, A.E., Burbank, D.W., Farley, K.A., and Fielding, E.J., 2000, Structural and topographic evolution of the central Transverse Ranges, California, from apatite fission-track, (U-Th)/He and digital elevation model analyses: Basin Research, v. 12, p. 97–114, doi: 10.1046/j.1365-2117.2000.00116.x.

Bogucki, D.J., 1976, Debris slides in the Mt. Le Conte area, Great Smoky Mountains National Park, U.S.A.: Geografiska Annaler, v. 58A, p. 179–191.

Brandon, M.T., Roden-Tice, M.K., and Garver, J.I., 1998, Late Cenozoic exhumation of the Cascadia accretionary wedge in the Olympic Mountains: NW Washington State: Geological Society of America Bulletin, v. 110, p. 985–1009, doi: 10.1130/0016-7606(1998)110<0985:LCEOTC>2.3.CO;2.

Brown, W.M., III, 1973, Erosion processes, fluvial sediment transport, and reservoir sedimentation in a part of the Newell and Zayante Creek basins, Santa Cruz County, California: U.S. Geological Survey Open-File Report 73-35, 31 p.

Campbell, C.S., 1990, Rapid granular flows: Annual Review of Fluid Mechanics, v. 22, p. 57–92, doi: 10.1146/annurev.fl.22.010190.000421.

Cannon, S.H., 2001, Debris-flow generation from recently burned watersheds: Environmental and Engineering Geoscience, v. 7, p. 321–341.

Capart, H., Fraccarollo, L., Guarino, L., Armanini, A., and Zech, Y., 2000, Granular temperature behaviour of loose bed debris-flows, *in* Wieczorek, G., and Naeser, N., eds., Debris-flow hazards mitigation: Mechanics, prediction, and assessment: Rotterdam, Balkema, p. 361–368.

Cerling, T.E., Webb, R.H., Poreda, R.J., Rigby, A.D., and Melis, T.S., 1999, Cosmogenic ^{3}He ages and frequency of late Holocene debris flows from Prospect Canyon, Grand Canyon, USA: Geomorphology, v. 27, p. 93–111, doi: 10.1016/S0169-555X(98)00092-0.

Craig, K., Buckholtz, R.H., and Domoto, G., 1986, An experimental of the rapid flow of dry cohesionless metal powders: Transactions, ASME Journal of Applied Mechanics, v. 53, p. 935–942.

Craig, K., Buckholtz, R.H., and Domoto, G., 1987, The effects of shear surface boundaries on stresses for the rapid shear of dry powders: Transactions, ASME Journal of Tribology, v. 109, p. 232–237.

Cuogiang, O., Kobashi, S., and Mizuyama, T., 1993, Development processes of debris-flow: Journals of the Japan Society of Erosion Control Engineering, v. 46, p. 11–20.

Davies, T.R.H., 1990, Debris-flow surges—Experimental simulation: Journals of Hydrology (N.Z.), v. 29, p. 18–46.

Davis, F.D., 1983, Geologic map of the southern Wasatch Front, Utah: Utah Geological Survey Map 55-A, scale 1:100,000.

Deketh, H.J.R., Grima, M.A., Hergarden, I.M., Giezen, M., and Verhoef, P.N.W., 1998, Towards the prediction of rock excavation machine performance: Bulletin of Engineering Geology and the Environment, v. 57, p. 3–15, doi: 10.1007/s100640050016.

Dietrich, W.E., and Dunne, T., 1978, Sediment budget for a small catchment in mountainous terrain: Zeitschrift für Geomorphologie, v. 29, Supplement, p. 191–206.

Dietrich, W.E., Wilson, C.J., and Reneau, S.L., 1986, Hollows, colluvium, and landslides in soil-mantled landscapes, *in* Abrahams, A.D., ed., Hillslope processes: Winchester, Massachusetts, Allen and Unwin, p. 361–388.

Dietrich, W.E., Bellugi, D., Heimsath, A., Roering, J.J., Sklar, L., and Stock, J.D., 2003, Geomorphic transport laws for predicting landscape form and dynamics, *in* Wilcock, P.R., and Iverson, R.M., eds., Prediction in geomorphology: American Geophysical Union, Geophysical Monograph Series, v. 135, p. 103–132.

Eaton, L.S., Morgan, B.A., Kochel, R.C., and Howard, A.D., 2003, Role of debris flows in long-term landscape denudation in the central Appalachians of Virginia: Geology, v. 31, p. 339–342, doi: 10.1130/0091-7613(2003)031<0339:RODFIL>2.0.CO;2.

Evans, A.G., Gulden, M.E., and Rosenblatt, M., 1978, Impact damage in brittle materials in the elastic-plastic response regime: Proceedings of the Royal Society of London, Ser. A, v. 361, p. 343–365.

Finnie, I., 1960, Erosion of surfaces by solid particles: Wear, v. 3, p. 87–103, doi: 10.1016/0043-1648(60)90055-7.

Fowell, R.J., and Smith, I.M., 1976, Factors influencing the cutting performance of a selective tunneling machine, *in* Jones, M.J., ed., Tunnelling '76, proceedings of an international symposium: London, Institution of Mining and Metallurgy, p. 301–309.

Franklin, J.A., Broch, E., and Walton, G., 1971, Logging the mechanical character of rock: Transactions of the Institution of Mining and Metallurgy, Section B—Applied Earth Science, v. 80A, p. 1–9.

Gahr, K.-H.Z., 1987, Microstructure and wear of materials: Amsterdam, Elsevier, 560 p.

Gol'din, B.M., and Lyubashevskiy, L.S., 1966, Computation of the velocity of mudflows for Crimean rivers: Soviet Hydrology, Selected Paper 1966, no. 2, p. 179–181.

Goodman, R.E., 1980, Introduction to rock mechanics: New York, Wiley and Sons, 478 p.

Goretta, K.C., Burdt, M.L., Cuber, M.M., Perry, L.A., Singh, D., Wagh, A.S., Routbort, J.L., and Weber, W.J., 1999, Solid-particle erosion of portland cement and concrete: Wear, v. 224, p. 106–112, doi: 10.1016/S0043-1648(98)00339-1.

Haff, P., 1983, Grain flow as a fluid-mechanical phenomenon: Journal of Fluid Mechanics, v. 134, p. 401–430, doi: 10.1017/S0022112083003419.

Hanes, D.M., and Inman, D.L., 1985, Observations of rapidly flowing granular fluid flow: Journal of Fluid Mechanics, v. 150, p. 357–380, doi: 10.1017/S0022112085000167.

Harris, S.A., and McDermid, G., 1998, Frequency of debris flows on the Sheep Mountain fan, Kluane Lake, Yukon Territory: Zeitschrift für Geomorphologie, v. 42, p. 159–175.

Heimsath, A.M., Dietrich, W.E., Nishiizumi, K., and Finkel, R.C., 2001, Stochastic processes of soil production and transport: Erosion rates, topographic variation, and cosmogenic nuclides in the Oregon Coast Range: Earth Surface Processes and Landforms, v. 26, p. 531–552, doi: 10.1002/esp.209.

Hirano, M., and Iwamoto, M., 1981, Measurement of debris flow and sediment-laden flow using a conveyor-belt flume in a laboratory, *in* Davies, T.R.H., and Pearce, A.J., eds., Proceedings of International Symposium on Erosion and Sediment Transport in Pacific Rim Steeplands: International Association of Hydrological Sciences Publication 132, p. 225–230.

Hockey, B.J., Wiederhorn, S.M., and Johnson, H., 1978, Fracture mechanics of ceramics, v. 3, Flaws and testing: New York, Plenum Press, 506 p.

Howard, A.D., 1994, A detachment-limited model of drainage basin evolution: Water Resources Research, v. 30, p. 2261–2285.

Hsiau, S.-S., and Jang, H.-W., 1998, Measurements of velocity fluctuations of granular materials in a shear cell: Experimental Thermal and Fluid Science, v. 17, p. 202–209, doi: 10.1016/S0894-1777(97)10041-3.

Hsiau, S.-S., and Shieh, Y.-H., 1999, Fluctuations and self-diffusion of sheared granular material flows: Journal of Rheology, v. 43, p. 1049–1066, doi: 10.1122/1.551027.

Hsu, L., and Dietrich, W.E., 2004, Experimental study of surface erosion by granular flows: Eos (Transactions, American Geophysical Union), v. 85, p. 47.

Ikeya, H., 1981, A method of designation for area in danger of debris flow, *in* Davies, T.R.H., and Pearce, A.J., eds., Proceedings of International Symposium on Erosion and Sediment Transport in Pacific Rim Steeplands: International Association of Hydrological Sciences Publication 132, p. 576–588.

Ishikawa, Y., 1999, Morphological and geological features of debris flows caused by earthquakes: Journal of the Japan Society of Erosion Control Engineering, v. 51, p. 35–42.

Iverson, R.M., 1997, The physics of debris flows: Reviews in Geophysics, v. 35, p. 245–296, doi: 10.1029/97RG00426.

Iverson, R.M., and Denlinger, R.P., 2001, Flow of variably fluidized granular masses across three-dimensional terrain: Journal of Geophysical Research, v. 106, p. 537–552, doi: 10.1029/2000JB900329.

Iverson, R.M., and Major, J.J., 1986, Groundwater seepage vectors and the potential for hillslope failure and debris flow mobilization: Water Resources Research, v. 22, p. 1543–1548.

Iverson, R.M., and Vallance, J.W., 2001, New views of granular mass flows: Geology, v. 29, p. 115–118, doi: 10.1130/0091-7613(2001)029<0115:NVOGMF>2.0.CO;2.

Iverson, R.M., LaHusen, R.G., Major, J.J., and Zimmerman, C.L., 1994, Debris flow against obstacles and bends; dynamics and deposits: Eos (Transactions, American Geophysical Union), v. 75, p. 274.

Jaeger, J.C., and Cook, N.G.W., 1976, Fundamentals of rock mechanics: London, Chapman and Hall, 585 p.

Jenkins, J.T., and Savage, S.B., 1983, A theory for the rapid flow of identical, smooth, nearly elastic particles: Journal of Fluid Mechanics, v. 130, p. 187–202, doi: 10.1017/S0022112083001044.

Karpuz, C., Pasamehmetoglu, A.G., Bozdag, T., and Muftuoglu, Y., 1990, Rippability assessment in surface coal mining, *in* Singhal, R.K., and Vavra, M., eds., Proceedings of the Second International Symposium on Mine Planning and Equipment Selection: Calgary, Canada, p. 315–322.

Lague, D., and Davy, P., 2003, Constraints on the long-term colluvial erosion law by analyzing slope-area relationships at various tectonic uplift rates in the Siwaliks Hills (Nepal): Journal of Geophysical Research, v. 108, p. 2129, doi: 10.1029/2002JB001893, doi: 10.1029/2002JB001893.

Lhymn, C., and Wapner, P., 1987, Slurry erosion of polyphenylene sulfide-glass fiber composites: Wear, v. 119, p. 1–11, doi: 10.1016/0043-1648(87)90094-9.

Lo, K.Y., and Hefny, A.M., 2001, Basic rock mechanics and testing, Chapter 6, *in* Rowe, R.K., ed., Geotechnical and geoenvironmental engineering handbook: Boston, Kluwer, 1088 p.

Longo, S., and Lamberti, A., 2000, Granular streams rheology and mechanics: Physics and Chemistry of the Earth (B), v. 25, p. 375–380.

Lun, C.K.K., and Savage, S.B., 1986, The effects of an impact velocity dependent coefficient of restitution on stresses developed by sheared granular materials: Acta Mechanica, v. 63, p. 15–44, doi: 10.1007/BF01182538.

Major, J.J., and Iverson, R.M., 1999, Debris-flow deposition: Effects of pore-fluid pressure and friction concentrated at flow margins: Geological Society of America Bulletin, v. 111, p. 1424–1434, doi: 10.1130/0016-7606(1999)111<1424:DFDEOP>2.3.CO;2.

McTigue, D.F., 1982, A nonlinear constitutive model for granular materials: Application to gravity flow: Journal of Applied Mechanics, v. 49, p. 291–296.

Meng, H.C., and Ludema, K.C., 1995, Wear models and predictive equations: Their form and content: Wear, v. 181–183, p. 443–457, doi: 10.1016/0043-1648(95)90158-2.

Merritts, D., and Vincent, K.R., 1989, Geomorphic response of coastal streams to low, intermediate, and high rates of uplift, Mendocino triple junction region, northern California: Geological Society of America Bulletin, v. 101, p. 1373–1388, doi: 10.1130/0016-7606(1989)101<1373:GROCST>2.3.CO;2.

Meyer, G.A., Pierce, J.L., Wood, S.H., and Jull, A.J.T., 2001, Fires, storms, and sediment yield in the Idaho batholith: Hydrological Processes, v. 15, p. 3025–3038, doi: 10.1002/hyp.389.

Mizuyama, T., Kobashi, S., and Guogiang, O., 1993, Development of debris flow, *in* Hadley, R.F., and Mizuyama, T., eds., Sediment problems: Strategies for monitoring, prediction and control: Proceedings of the Yokohama Symposium, International Association of Hydrological Sciences Publication 217, p. 141–145.

Montgomery, D.R., and Foufoula-Georgiou, E., 1993, Channel network source representation using digital elevation models: Water Resources Research, v. 29, p. 3925–3934, doi: 10.1029/93WR02463.

Nakashima, T., 1986, Experimental study on the motion of debris flow heads: Shin-Sabo, v. 39, p. 15–22.

Neilson, J.H., and Gilchrist, A., 1968, Erosion by a stream of solid particles: Wear, v. 11, p. 111–122, doi: 10.1016/0043-1648(68)90591-7.

Ogawa, S., 1978, Multi-temperature theory of granular materials, *in* Cowin, S.C., and Satake, M., eds., Proceedings of the US-Japan Seminar on Continuum-Mechanical and Statistical Approaches in the Mechanics of Granular Materials, Tokyo: Tokyo, Gakujutsu Bunken Fukyukai, p. 207–217.

Okuda, S., Suwa, H., Okunishi, K., Nakano, M., and Yokoyama, K., 1977, Synthetic observation on debris flow, Part 3, Observation at valley Kamikamihorizawa of Mt. Yakedake in 1976: Disaster Prevention Research Institute Annuals, Kyoto University, v. 20B-1, p. 237–263.

Okuda, S., Suwa, H., Okunishi, K., Yokoyama, K., Nakano, M., Ogawa, K., and Hamana, S., 1978, Synthetic observation on debris flow, Part 4, Observation at valley Kamikamihorizawa of Mt. Yakedake in 1977: Disaster Prevention Research Institute Annuals, Kyoto University, v. 21B-1, p. 277–296.

Okuda, S., Suwa, H., Okunishi, K., Yokoyama, K., Ogawa, K., and Hamana, S., 1979, Synthetic observation on debris flow, Part 5, Observation at valley Kamikamihorizawa of Mt. Yakedake in 1978: Disaster Prevention Research Institute Annuals, Kyoto University, v. 22, p. 157–204.

Okuda, S., Suwa, H., Okunishi, K., Yokoyama, K., Ogawa, K., Hamana, S., and Tanaka, K., 1980a, Synthetic observation on debris flow, Part 6, Observation at valley Kamikamihorizawa of Mt. Yakedake in 1979: Disaster Prevention Research Institute Annuals, Kyoto University, v. 23, p. 357–394.

Okuda, S., Suwa, H., Okunishi, K., Yokoyama, K., and Nakano, M., 1980b, Observations on the motion of a debris flow and its geomorphological effects: Zeitschrift für Geomorphologie: Suppl-Bd. v. 35, p. 142–163.

Okuda, S., Suwa, H., Okunishi, K., Yokoyama, K., and Ogawa, K., 1981, Synthetic observation on debris flow, Part 7, Observation at valley Kamikamihorizawa of Mt. Yakedake in 1980: Disaster Prevention Research Institute Annuals, Kyoto University, v. 24, p. 411–448.

Orme, A.R., 1990, Recurrence of debris production under coniferous forest, Cascade foothills, northwest United States, *in* Thornes, J.B., ed., Vegetation and erosion: New York, Wiley and Sons, p. 67–84.

Perg, L., Anderson, R.S., and Finkel, R., 2000, Cosmogenic radionuclide constraints on the long-term sediment budget of the Santa Cruz littoral cell, California, US: Eos (Transactions, American Geophysical Union), v. 81, p. 27, 28.

Personius, S.F., 1995, Late Quaternary stream incision and uplift in the forearc of the Cascadia subduction zone, western Oregon: Journal of Geophysical Research, v. 100, p. 20,193–20,210, doi: 10.1029/95JB01684.

Pettifer, G.S., and Fookes, P.G., 1994, A revision of the graphical method for assessing the excavatability of rock: Quarterly Journal of Engineering Geology, v. 27, p. 145–164.

Pomeroy, J.S., 1980, Storm-induced debris avalanching and related phenomenon in the Johnstown area, Pennsylvania, with references to other studies in the Appalachians: U.S. Geological Survey Professional Paper 1191, 24 p.

Reneau, S.L., and Dietrich, W.E., 1987, The importance of hollows in debris flow studies: Examples from Marin County, California, *in* Costa, J.E., and Wieczorek, G.F., eds., Debris flows/avalanches: Process, recognition, and mitigation: Geological Society of America Reviews in Engineering Geology, v. 7, p. 165–180.

Reneau, S.L., and Dietrich, W.E., 1991, Erosion rates in the southern Oregon Coast Range: Evidence for equilibrium between hillslope erosion and sediment yield: Earth Surface Processes and Landforms, v. 16, p. 307–322.

Roering, J.J., Kirchner, J.W., and Dietrich, W.E., 1996, Identification and characterization of deep-seated landslides in the Oregon Coast Range using digital terrain data: Eos (Transactions, American Geophysical Union), v. 77, p. 246.

Roering, J.J., Schmidt, K.M., Stock, J.D., Dietrich, W.E., and Montgomery, D.R., 2003, Shallow landsliding, root reinforcement, and the spatial distribution of trees in the Oregon Coast Ranges: Canadian Geotechnical Journal, v. 40, p. 237–253, doi: 10.1139/t02-113.

Routbort, J.L., Scattergood, R.O., and Kay, E.W., 1980, Erosion of silicon single crystals: Journal of the American Ceramic Society, v. 63, p. 635–640.

Ryu, I.-C., Niem, A.R., and Niem, W.A., 1996, Oil and gas potential of the southern Tyee Basin: Southern Oregon Coast Range: Oregon Department of Geology and Mineral Industries, Oil and Gas Investigation 19, 141 p.

Sabo Publicity Center, 1988, Debris flow at Sakurajima, Japan: Japan, Ministry of Construction, 65 p.

Savage, S.B., and Hutter, K., 1989, The motion of a finite mass of granular material down a rough incline: Journal of Fluid Mechanics, v. 199, p. 177–215, doi: 10.1017/S0022112089000340.

Savage, S.B., and McKeown, S., 1983, Shear stresses developed during rapid shear of concentrated suspensions of large spherical particles between concentric cylinders: Journal of Fluid Mechanics, v. 127, p. 453–472, doi: 10.1017/S0022112083002827.

Savage, S.B., and Sayed, M., 1984, Stresses developed in dry cohesionless granular materials sheared in an annular shear cell: Journal of Fluid Mechanics, v. 142, p. 391–430, doi: 10.1017/S0022112084001166.

Schmidt, K.M., Roering, J.J., Stock, J.D., Dietrich, W.E., Montgomery, D.R., and Schaub, T., 2001, The variability of root cohesion as an influence on shallow landslide susceptibility in the Oregon Coast Range: Canadian Geotechnical Journal, v. 38, p. 995–1024, doi: 10.1139/cgj-38-5-995.

Seidl, M.A., and Dietrich, W.E., 1992, The problem of channel erosion into bedrock, *in* Schmidt, K.-H., and DePloey, J., eds., Functional geomorphology: Catena-Verlag Rohdenburg, Cremlingen-Destedt, Federal Republic of Germany (DEU) Supplement 23, p. 101–124.

Selby, M.J., 1980, A rock mass strength classification for geomorphic purposes: With tests from Antarctica and New Zealand: Zeitschrift für Geomorphologie, v. 24, p. 31–51.

Sheldon, G.L., and Finnie, I., 1966, The mechanism of material removal in the erosive cutting of brittle materials: Transactions, ASME Journal of Engineering for Industry, v. 88, p. 393–400.

Sheldon, G.L., and Kanhere, A., 1972, An investigation of impingement erosion using single particles: Wear, v. 21, p. 195–209, doi: 10.1016/0043-1648(72)90257-8.

Sklar, L., and Dietrich, W.E., 1998, River longitudinal profiles and bedrock incision models; stream power and the influence of sediment supply, *in* Tinkler, K.J., and Wohl, E.E., eds., Rivers over rock; fluvial processes in bedrock channels: Washington, D.C., American Geophysical Union Geophysical Monograph, v. 107, p. 237–260.

Sklar, L.S., and Dietrich, W.E., 2001, Sediment and rock strength controls on river incision into bedrock: Geology, v. 29, p. 1087–1090, doi: 10.1130/0091-7613(2001)029<1087:SARSCO>2.0.CO;2.

Snyder, N.P., Whipple, K.X, Tucker, G.E., and Merritts, D.J., 2000, Landscape response to tectonic forcing: Digital elevation model analysis of stream profiles in the Mendocino triple junction region, northern California: Geological Society of America Bulletin, v. 112, p. 1250–1263, doi: 10.1130/0016-7606(2000)112<1250:LRTTFD>2.3.CO;2.

Spotila, J.A., Farley, K.A., Yule, J.D., and Reiners, P.W., 1999, Rapid, long-lived exhumation along the transpressive San Andreas Fault Zone in Southern California, based on U-Th/He dating: Eos (Transactions, American Geophysical Union), v. 80, p. F1170.

Stack, M.M., Corlett, N., and Zhou, S., 1999, Impact angle effects on the transition boundaries of the aqueous erosion-corrosion map: Wear, v. 225–229, p. 190–198, doi: 10.1016/S0043-1648(99)00050-2.

Stephenson, R., 1984, Flexural models of continental lithosphere based on the long-term erosional decay of topography: Geophysical Journal of the Royal Astronomical Society, v. 77, p. 385–413.

Stock, J.D., 2003, Incision of steepland valleys by debris flows [Ph.D. thesis]: Berkeley, University of California, 245 p.

Stock, J.D., and Dietrich, W.E., 2003, Valley incision by debris flows: Evidence of a topographic signature: Water Resources Research, v. 39, doi: 10.1029/2001WR001057, doi: 10.1029/2001WR001057.

Stock, J.D., and Montgomery, D.R., 1999, Geologic constraints on bedrock river incision using the stream power law: Journal of Geophysical Research, v. 104, p. 4983–4993, doi: 10.1029/98JB02139.

Stock, J.D., Montgomery, D.R., Collins, B.D., Dietrich, W.E., and Sklar, L., 2005, Field measurements of incision rates following bedrock exposure: Implications for process controls on the long-profiles of valleys cut by rivers and debris flows: Geological Society of America Bulletin, v. 117, p. 174–194, doi: 10.1130/B25560.1.

Suwa, H., and Okuda, S., 1980, Dissection of valleys by debris flows: Zeitschrift für Geomorphologie, v. 35, Supplement, p. 164–182.

Suwa, H., and Okuda, S., 1983, Deposition of debris flows on a fan surface, Mt. Yakedake, Japan: Zeitschrift für Geomorphologie, v. 46, Supplement, p. 79–101.

Suwa, H., and Yamakoshi, T., 2000, Estimation of debris-flow motion by field surveys, *in* Wieczorek, G., and Naeser, N., eds., Debris-flow hazards mitigation: Mechanics, prediction, and assessment: Rotterdam, Balkema, p. 293–299.

Suwa, H., Okuda, S., and Ogawa, K., 1984, Size segregation of solid particles in debris flows, Part 1: Accumulation of large boulders at the flow front and inverse grading by kinetic sieving effect: Disaster Prevention Research Institute Annuals, Kyoto University, v. 27, p. 409–423.

Suwa, H., Okunishi, K., and Sakai, M., 1993, Motion, debris size and scale of debris flows in a valley on Mount Yakedake, Japan, *in* Hadley, R.F., and Mizuyama, T., eds., Proceedings, Sediment problems: Strategies for monitoring, prediction and control: Yokohama, International Association of Hydrological Sciences Publication 217, p. 239–248.

Taylor, E.D., and Hunt, M.L., 1993, Measurements of velocity fluctuations in a granular flow, *in* Thornton, C., ed., Powders and grains 93: Rotterdam, Balkema, p. 275–279.

Thuro, K., 1997, Drillability prediction: Geological influences in hard rock drill and blast tunneling: Geologische Rundschau, v. 86, p. 426–438, doi: 10.1007/s005310050151.

Thuro, K., and Plinninger, R.J., 1999, Roadheader excavation performance—Geological and geotechnical influences, *in* Vouille, G., and Berest, P., eds., 9th International Conference on Rock Mechanics, Paris: Rotterdam, Balkema, p. 1241–1244.

Vervoort, A., and De Wit, K., 1997, Correlation between dredgeability and mechanical properties of rock: Engineering Geology, v. 47, p. 259–267, doi: 10.1016/S0013-7952(97)00023-9.

Vutukuri, V.S., Lama, R.D., and Saluja, S.S., 1974, Handbook on mechanical properties of rocks, Volume 1: Testing techniques and results: Rockport, Massachusetts, Bay Village Ohio, Transactions, Technical Publications, p. 105–115.

Walker, G.W., and MacLeod, N.S., 1991, Geologic Map of Oregon: U.S. Geological Survey, scale 1:500,000, 2 sheets.

Watanabe, M., and Ikeya, H., 1981, Investigation and analysis of volcanic mud flows on Mt. Sakurajima, *in* Walling, D.E., and Tacconi, P., eds., Proceedings, Symposium on Erosion and Sediment Transport Measurement: Florence, International Association of Hydrological Sciences Publication 133, p. 245–256.

Wiederhorn, S.M., and Hockey, B.J., 1983, Effect of material parameters on the erosion resistance of brittle materials: Journal of Materials Science, v. 18, p. 766–780, doi: 10.1007/BF00745575.

Wiederhorn, S.M., and Lawn, B.R., 1979, Strength degradation of glass impacted with sharp particles: I: Journal of the American Ceramic Society, v. 62, p. 66–70.

Whipple, K.X, and Tucker, G.E., 1999, Dynamics of the stream-power river incision model; implications for height limits of mountain ranges, landscape response timescales, and research needs: Journal of Geophysical Research, v. 104, p. 17,661–17,674, doi: 10.1029/1999JB900120.

Wieczorek, G.F., Morgan, B.A., and Campbell, R.H., 2000, Debris-flow hazards in the Blue Ridge of Central Virginia: Environmental and Engineering Geoscience, v. 6, p. 3–23.

Williams, G.P., and Guy, H.P., 1973, Erosional and depositional aspects of Hurricane Camille in Virginia, 1969: U.S. Geological Survey Professional Paper 804, 80 p.

Woodruff, J.F., 1971, Debris avalanches as an erosional agent in the Appalachian Mountains: Journal of Geography, v. 70, p. 399–406.

Yoshida, K., Kikuchi, S.-I., Nakamura, F., and Noda, M., 1997, Dendrochronological analysis of debris flow disturbance on Rishiri Island: Geomorphology, v. 20, p. 135–145, doi: 10.1016/S0169-555X(97)00010-X.

Manuscript Received 26 September 2005
Revised Manuscript Received 3 April 2006
Manuscript Accepted 30 April 2006

Printed in the USA